Climate Dynamics (1990) 4:95–125

Climate Dynamics

Ocean-circulation model of the carbon cycle

R Bacastow[1] **and E Maier-Reimer**[2]

[1] Scripps Institution of Oceanography, San Diego, La Jolla, CA 92093, USA
[2] Max-Planck-Institut für Meteorologie, D-2000 Hamburg 13, Federal Republic of Germany

Received March 23, 1988/Accepted October 16, 1989

Abstract. A three-dimensional model of the natural carbon cycle in the oceans is described. The model is an extension of the inorganic ocean-circulation carbon cycle model of Maier-Reimer and Hasselmann (1987) to include the effect of the ocean biota. It is based on a dynamic, general circulation model of the world oceans. Chemical species important to the carbon cycle are advected by the current field of the general circulation model. Mixing occurs through numerical diffusivity (related to finite box size), a small explicit horizontal diffusivity, and a convective adjustment. An atmospheric box exchanges CO_2 with the surface ocean. There is no land biota provided in the present version of the model. The effect of the ocean biota on ocean chemistry is represented in a simple way and model distributions of chemical species are compared with distributions observed during the GEOSECS and other expeditions.

Introduction

Relatively simple one-dimensional models and box models with a small number of boxes have long been used to model the oceanic carbon cycle. Such models might be termed analogue models because they relate transport of CO_2 to that of other tracers, most commonly ^{14}C [for a review of these models, see Bacastow and Björkström (1981)]. The structure of the oceans in analogue models is extremely simple and processes by which transport takes place may be quite different from those in the real ocean. For example, vertical transport that probably takes place largely by advection along nearly horizontal isopycnal surfaces is typically modeled by vertical eddy diffusion (Oeschger et al. 1975). It is thought that calibration by ^{14}C and ^{3}H mostly compensates for this difference in mechanism. Validation of analogue models is difficult, however, because they make few significant predictions beyond those needed to set parameters in the model. Estimates of the uptake of fossil fuel CO_2 since the beginning of the industrial revolution, and predictions of uptake for various future scenarios, have been mainly based on analogue models.

Development of a better ocean model is important. Chemical oceanographers, using analogue models calibrated by ^{14}C, would have the land biota a small sink for fossil fuel of approximately 0.5 gt C year^{-1} (where 1 gt C = 10^{15} g of carbon), from atmospheric measurements and fossil fuel production data. Biologists, in general, would have the land biota a source to the atmosphere of 0.4–4.7 gt C year^{-1} (Houghton et al. 1983; Detwiler and Hall 1988), from direct observation of land clearing, especially in the tropics.

A better oceanic model should realistically depict large departures from the steady-state, natural carbon cycle. A representation of first-order perturbations, as in most analogue models, will be less and less adequate as atmospheric CO_2 increases. Also, there is a need to understand the reason for the decrease in atmospheric CO_2 concentration that accompanied the last ice age, and so-called feedback effects that might accompany a CO_2-induced warmer climate.

Measurements of CO_2 in ice cores indicate that the atmospheric CO_2 level rose about 70 ppm at the close of the last glacial epoch (Neftel et al. 1982; Delmas et al. 1980). This change in CO_2 concentration may have been caused by a change in ocean circulation, through a relation between ocean cir-

Offprint requests to: R Bacastow

culation, the ocean biota, and ocean chemistry (Siegenthaler and Wenk 1984; Sarmiento and Toggweiler 1984; Knox and McElroy 1984).

A large part of the downward transport of carbon in the oceans is related to life processes. Photosynthesis occurs in a near-surface euphotic layer. Fecal pellets, shell parts, and other organic debris sink or are carried by the current field to deeper water, where they partially decompose and dissolve. The nutrients released in this way in below-surface waters are then returned to the surface by ocean circulation and mixing. Very low concentrations of the nutrients phosphorous and nitrogen in much of the ocean's surface water indicate that photosynthesis is limited in these regions by the rate of return of nutrients. Much higher concentrations in upwelling regions, particularly in the Antarctic and Arctic, and along the Equator, are suggestive that other factors may limit photosynthesis there.

The better ocean model that we seek should function in a realistic way — the mechanisms of transport should be the same as those in the real ocean. There is an intimate relationship between ocean circulation, life processes in the ocean, and atmospheric CO_2 level. We must understand this relationship if we are to have confidence in the predictions of our models for the uptake of anthropogenic CO_2.

The development of three-dimensional oceanic general circulation models (oceanic GCMs), and the recent increased availability of very fast computers, has opened a new approach to modeling the oceanic carbon cycle. With transport of chemical species provided by the circulation field, the exchange of CO_2 between the atmosphere and the oceans, and the effects of the ocean biota can be modeled far more realistically than is possible with one-dimensional models. Also, oceanic GCM based models make many detailed predictions of spatial and temporal features of tracers and other chemical species which can be systematically compared to observations.

The model described here is an extension of the inorganic ocean-circulation carbon cycle model of Maier-Reimer and Hasselmann (1987) (hereafter referred to as MRH) to include a first-order representation of the effects of the ocean biota.

Model description

Ocean general circulation model

The carbon cycle model is based on a numerical ocean-circulation model designed for climate studies (Maier-Reimer et al. 1982; Maier-Reimer and Hasselmann 1987). The circulation model is a preliminary version of a model proposed by Hasselmann (1982). The model is driven by observationally derived surface winds, and salinity and temperature are held close to observational values at the ocean surface. The grid is coarse, about 555 km between points near the Equator, and the time step, 1 month, is long. Ocean bathymetry is realistic, within the limitations imposed by the grid. Many small-scale features, such as the English Channel and the Mediterranean Sea, are lost entirely. Only two "islands", Australia and Antarctica, survive.

The equations of motion have been filtered to eliminate gravity waves and are divided into barotropic and baroclinic parts. The solution of the barotropic part is obtained in a quasi-static, near-geostrophic approximation by use of a potential function. The baroclinic solution is essentially an advection of the temperature and salinity fields. The density field is then re-evaluated in preparation for the next barotropic solution. The motion may be described as frictional geostrophy; deviations from geostrophy are propagated by Rossby waves. The model runs about an order of magnitude faster than primitive equation models.

The model successfully reproduces large-scale horizontal features of ocean circulation — for example, the Gulf Stream and the mid-latitude gyres. The major ingredients of the thermohaline circulation are included in the model, but deep water formation does not seem to be as concentrated in the North Atlantic as in the real ocean.

The circulation model provides ten vertical levels of computation, at 75, 150, 250, 450, 700, 1000, 2000, 3000, 4000, and 5000 m below the surface, and each level is discretized by a 72×72 grid. The grid is "staggered", as in Fig. 1: "vector" points, indicated by ($\times$), alternate with "scalar" points, indicated by ($+$). This E-type staggering (Arakawa and Lamb 1977) has severe disadvantages for representing gravity waves and consequently is rarely used. For implementing the geostrophic approximation, however, it may be more appropriate than other grids. Velocity components u (zonal) and v (meridional) are evaluated only at vector points, and temperature, salinity, and pressure are evaluated only at scalar points. Comparable points are thus separated by 5° in both meridional and zonal directions. The vertical velocity components w are calculated at levels half-way between the computational levels, at the horizontal locations of the scalar points, from the equation for conservation of water.

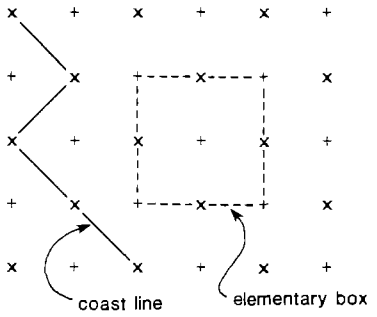

Fig. 1. Plan view of grid. Horizontal velocities exist at vector points, denoted by *crosses* (×), and pressure, temperature, salinity, and concentration exist at scalar points, denoted by *pluses* (+). Water depth is fixed at vector points, so coastlines go through vector points, as indicated. The elementary box associated with a scalar point is shown

Water depth is specified at vector points. Thus the coastlines go through vector points, as in Fig. 1. At scalar points, the water depth is defined to be the maximum of the four surrounding vector points, so that a substance can always be advected from one "wet" scalar point to a neighboring "wet" scalar point by the velocity at a "wet" vector point between them.

Four scalar points surround each scalar point, and together with the levels at which w is defined, naturally divide the ocean into boxes (Fig. 1). The four surrounding scalar points define the vertical corners of the box, and the top and bottom are taken to be horizontal at the level of the w points. The deepest of the boxes in each vertical stack extends to the bottom of the ocean at the central scalar point, i.e. from a w level half-way between the two lowest "wet" computational levels to the maximum depth of the four surrounding vector points. The lowest boxes, then, have varying height. The change in the ocean depth between boxes may be thought of as taking place very close to vector points. In this way, the ocean is represented by 27443 boxes.

It is immediately evident that these boxes overlap horizontally, so that if one were to sum all the water in them one would obtain approximately twice the water in the ocean. One must divide such a sum by 2.

The model does not attempt to determine the depth of the wind-mixed layer from physical principles. This depth is consequently set arbitrarily to the depth of the surface box, 112.5 m, which corresponds roughly to the winter depth of the observed wind-mixed layer in the Northern Pacific (Bathen 1972). The effective wind-mixed layer is deepened at certain points by the convective adjustment described below.

The model is closed at the North Pole by assuming a small island there. The two rows of vector points closest to the North Pole, at latitudes 88.75° and 86.25°, are forced to be "dry", and the box thicknesses at the northern most scalar points, at 88.75°, are set to zero. This approximation should have no discernible effect on the circulation in the bulk of the ocean further south.

Carbon cycle model

Chemical concentrations are assigned to scalar points and are defined to be the average concentrations in the associated box. One may then think of the model as consisting of two oceans, and actual concentrations are represented by the average of the two oceans. With the simple "up-wind" advection scheme that is employed, the two oceans are not directly coupled by advection and consequently the solutions would be expected to be slightly different in the two oceans; to prevent this, a horizontal diffusivity of 1×10^6 cm^2 s^{-1} has been provided between neighboring points in the two oceans as indicated in the Appendix. Model runs with trial values of this diffusivity show significant change in Δ^{14}C section contours for much higher diffusivities (such as 1×10^7 cm^2 s^{-1}); lower values (0–1×10^5 cm^2 s^{-1}) lead to jagged contours which, after smoothing, agree well with the contours generated with a horizontal diffusivity of 1×10^6 cm^2 s^{-1}.

In a carbon cycle model it is important that chemical substances be conserved in the sense that any loss from one box must appear in another box. This requirement may be stated as

$$\sum_b C_b \Delta V_b = \text{constant}, \tag{1}$$

where the sum is over all boxes, C_b is the concentration in box b, and ΔV_b is the volume of the box. This has been accomplished by arranging the advective-diffusive numerical scheme so that all exchanges between boxes occur by fluxes across surfaces between boxes (see the Appendix).

The circulation model includes seasonal variation and employs a 1-month time step. It is integrated for a model time long enough for model variables to come to a dynamic steady state — about 5000 years. The carbon cycle model in its presents state of development, however, employs seasonally averaged results from the circulation model.

There is a convective adjustment in both the circulation and carbon cycle models. If any box of the circulation model develops a density greater than the box immediately below, it is mixed with that box. The location of this mixing is remembered, and these boxes are mixed at the beginning of each year duning a carbon cycle model run.

In the carbon cycle model, the atmosphere is represented by a well-mixed box of a size such that 290 ppm of CO_2 corresponds to 615.6×10^{15} g C. It exchanges CO_2 with the surface of the ocean through what may be taken to be a thin, resistive film at the ocean surface (Broecker and Peng 1982, p 113):

$$\frac{\Delta P_a}{\Delta t} = \sum_s \frac{k}{A_{oc}} (P_s - P_a) a_s. \quad (2)$$

Here P_a is the partial pressure of atmospheric CO_2, P_s is the partial pressure of CO_2 corresponding to values at the central scalar point of the surface box s, with surface area a_s, and the sum is over all "ice-free" ocean surface boxes. The total ice-free area is A_{oc}. The atmospheric exchange time with respect to the ocean, $1/k$, is taken to be 8 years. This corresponds to an average exchange flux of approximately 18 moles m^{-2} $year^{-1}$ (where the value of A_{oc} given below has been used).

Ice-free is assumed to mean a seasonally averaged temperature greater than $-1.7°$ C. There is some uncertainty in what should be considered ice-free, due to averaging the seasonal model results, and because some ocean areas contain both ice and open water. According to the above definition, the total ice-free surface area in the model, A_{oc}, is 352.1×10^6 km^2, and an additional ocean surface area of 1.2×10^6 km^2 is covered by ice.

The surface partial pressure of CO_2, P_s, is calculated from the temperature, total CO_2, alkalinity, and salinity concentrations of the surface box. The algorithm is from Bacastow (1981); the equilibrium constants for dissociation of carbonic acid, K_1 and K_2, are from an analysis of data of Hansson and of Mehrbach (Dickson and Millero 1987); the carbon dioxide solubility, K_0, is from Weiss (1974). The concentration of CO_2 in each surface box is adjusted for CO_2 transferred to or from the atmosphere. This procedure is equivalent to considering the ocean to be vertically mixed to the depth of the surface box, 112.5 m.

Ocean biota model

The coarse space and time scale of the carbon cycle model constrains the level of detail that can be resolved in the biota part of the model. Models of phytoplankton blooms and the chemical changes that accompany them may be quite complex [see, for example, Wroblewski (1977); Walsh (1975); Radach and Maier-Reimer (1975)]. However, phytoplankton blooms typically occur on a time scale measured in days or weeks. The coarse resolution leads to great simplification.

On a time scale of 1 year, the effect of the ocean biota is to cast downward CO_2, alkalinity, and nutrients from the surface water to lower depths. This coarse time scale is appropriate for ocean chemistry for depths below a few hundred meters. Concentrations there are found to be stable from year to year.

Much of this downward flux is in relatively large aggregates — fecal pellets and so-called marine snow — which sink at a rate which would take them to the bottom in a time short compared to the time required to be advected to another stack of boxes (Honjo et al. 1982). Smaller particles and dissolved organic carbon, which are advected with the current field, may also play a role, but they are now neglected.

The effect of the marine biota on ocean chemical concentrations is modeled. The model is about as simple as possible and still include what seem to be the most important mechanisms. Our objective is to form a basis from which improvements can be made. The essential concentrations modeled are total CO_2, alkalinity, phosphate and dissolved oxygen. Radiocarbon and ^{13}C are included for diagnostic purposes. Oxygen also would be diagnostic were it not that its concentration is required to remain non-negative. The "generalized" Redfield ratios listed in Table 1 are assumed to hold for the chemical changes associated with photosynthesis of organic matter and its subsequent remineralization. Soft tissue and hard tissue, such as shell debris, are considered separately.

Most primary production is recycled in the surface water near where it was formed. A portion of primary production, called new production (Eppley and Peterson 1979) is transported to deeper water where it is remineralized. It is the new production that must be modeled.

Photosynthesis is assumed limited to the surface boxes, 112.5 m thick, and the CO_2 concentration is reduced during each year due to soft-tissue formation in each surface box not covered by ice by the rate of new production, $PRODC$ mol kg^{-1} $year^{-1}$, which depends on a latitudinally varying incident light factor, LC, and the phosphate con-

centration PO4 through Michaelis-Menton kinetics (cf. Dugdale 1967):

$$PRODC = LC \cdot \frac{R \cdot RC \cdot \mathrm{PO4}}{H + RC \cdot \mathrm{PO4}}, \quad (3)$$

where RC is the carbon to phosphate Redfield ratio (105, see Table 1). Here R and H are adjustable parameters. Since the concentration of nitrate is also assumed related to phosphate by a Redfield ratio, $PRODC$ would be unchanged if the nitrate concentration NO3 were instead assumed to be the limiting nutrient. Then $RC \cdot$ PO4 would be replaced by $(RC/RN) \cdot$ NO3, where RN is the nitrate to phosphate Redfield ratio (see Table 1).

Table 1. Summary of parameter values for the standard case model

Stoichiometry quantities assumed in synthesis and decomposition of marine soft tissue (generalized Redfield ratios) (Broecker and Peng 1982):

C:N:P:O2 = RC:RN:1:RO = 105:15:1:135

Average concentrations		
Ocean akalinity	2373 μ eq l^{-1}	
Ocean total CO_2	2217 μ mol l^{-1}	
Ocean phosphate	2.145 μ eq l^{-1}	
Constants		
R	see Eq. (3)	20 μ mol l^{-1}
H	see Eq. (3)	40 μ mol l^{-1}
PA	ratio of carbon in hard tissue to soft tissue	0.15
τ_{am}	atmospheric exchange time	8.0 years
α_{am}	^{13}C fractionation coef., atm. to ocean	1.0
α_{mb}	^{13}C fractionation coef., ocean to soft tissue	0.982
α_{mc}	^{13}C fractionation coef., ocean to hard tissue	1.0

Incident light factor LC(latitude), assumed symetric about equator

Latitude (degrees)	LC
88.75	0.3420
86.25	0.3443
83.75	0.3487
81.25	0.3554
78.75	0.3644
76.25	0.3761
73.75	0.3905
71.25	0.4082
68.75	0.4289
66.25	0.4527
63.75	0.4791
61.25	0.5078
58.75	0.5382
56.25	0.5696
53.75	0.6016
51.25	0.6336
48.75	0.6652
46.25	0.6960
43.75	0.7259
41.25	0.7549
38.75	0.7826
36.25	0.8091
33.75	0.8341
31.25	0.8575
28.75	0.8792
26.25	0.8992
23.75	0.9174
21.25	0.9339
18.75	0.9487
16.25	0.9616
13.75	0.9726
11.25	0.9818
8.75	0.9891
6.25	0.9946
3.75	0.9982
1.25	1.0000
−1.25	1.0000
−3.75	0.9982 etc.

Remineralization coefficients for soft tissue $DMIN(K)$ and hard tissue $DISCA(K)$ specify fraction of entering flux that is converted from particulate matter to dissolved matter in box level K, where $K = 1$ refers to the surface layer.

K	DMIN(K)	$DISCA(K)$
1	—	—
2	0.1175	0.0
3	0.1929	0.0
4	0.2749	0.0
5	0.3249	0.0
6	0.6049	0.200
7	0.7603	0.400
8	0.7603	0.600
9	0.7603	0.600
10	1.000	1.000

The incident light factor LC (Table 1) includes a solar radiation factor (Holtslag and Van Ulden 1983, p 518–519)

$$K_0^+ = a_1 \sin\phi + a_2 \quad (4)$$

dependent on the solar elevation angle ϕ and atmospheric attenuation coefficients a_1 and a_2, which have been assigned the values 990 and -30 W m^{-2}, respectively. The solar elevation angle was calculated by a formula given by Holtslag and Van Ulden (1983, p 528). An additional fac-

tor, of less importance, was included for variation of transmittance into the ocean with solar elevation (Defant 1961, p 58), by assuming the ocean surface to be smooth. The incident light factor is the product of these two factors averaged over 1 year and normalized to unity at the grid points located at $\pm 1.25°$ latitude.

There is thus a downward flux from each surface box s of $(PRODC)_s \cdot \rho \Delta V_s$ moles C year^{-1} in soft tissue, where $\rho \Delta V_s$ is the "volume" of the box in kg of seawater. A fraction $DMIN(K)$ of this downward flux is assumed to remineralize in the K level box below the surface box s (K varies downward from 1 to 10), provided there is enough oxygen in this box. If not, only an amount is remineralized such that the oxygen concentration is reduced to zero. If the ocean bottom is encountered in some box other than 10, all the remaining flux is remineralized in this bottom box, provided again that there is enough oxygen. If there is flux left over after the oxygen in the bottom box is exhausted, the remaining flux is returned to the surface box. Although this is not perhaps the best possible place for it, the circumstance only rarely occurs. At present, $DMIN(K)$ is required to be the same everywhere in the ocean; thus only one set of values for $DMIN(K)$ must be selected.

An additional flux of calcium carbonate from hard tissue, of $(PRODC)_s \cdot \rho \Delta V_s \cdot PA$ moles per year, is assumed to sink from each surface box, in association with the soft-tissue carbon flux, where PA, ordinarily set to 0.15, is a factor relating the flux of carbon in hard tissue to that in soft tissue. The total CO_2 and alkalinity concentrations in the surface box are reduced by, respectively, $(PRODC)_s \cdot PA$ and $2 \cdot (PRODC)_s \cdot PA$, on this account. A fraction $DISCA(K)$ of the sinking carbonate flux is assumed to dissolve in the K level box beneath the surface box. Like $DMIN(K)$, $DISCA(K)$ is required to be the same everywhere in the ocean.

The alkalinity of the surface box is additionally increased by $(PRODC)_s \cdot RN/RC$, due to the effect of nitrate uptake in photosynthesis (the smaller contribution of phosphate has been neglected) (Brewer et al. 1975). Corresponding reductions in alkalinity take place in the boxes where soft tissue remineralizes.

The surface concentration of dissolved oxygen is set to 3% supersaturation (Broecker and Peng 1982, p 129). The saturation value is from Weiss (1970). If convective mixing of the top two boxes is called for, then the oxygen concentration in both boxes is adjusted as above. In boxes beneath the surface, remineralization of the carbon flux is accompanied by a reduction in oxygen concentration corresponding to its Redfield ratio (Table 1).

Radiocarbon is transported in the same way as stable carbon. An atmospheric source adds $^{14}CO_2$ to the atmospheric box, which exchanges $^{14}CO_2$ with each surface box of the ocean through an equation like Eq. (2). The partial pressure of $^{14}CO_2$ exerted by the surface ocean is assumed to be the same as for CO_2 but reduced by the ratio of total $^{14}CO_2$ to total CO_2 in the surface box. Total $^{14}CO_2$ is advected like other chemical species, but decays with a mean lifetime of 8267 years. It is incorporated in photosynthesised tissue, both soft and hard, in proportion to its concentration relative to total CO_2 in the surface box. The concentration of $^{14}CO_2$ is increased in boxes where remineralization of soft tissue and dissolution of hard tissue takes place. Implicit in this procedure is the very good approximation that $^{14}CO_2$ is too small in amount to affect the partial pressure of total CO_2 and that ^{14}C rapidly distributes throughout the total carbon pool. Fractionation has been omitted since ^{14}C results are compared to measurements in the $\Delta^{14}C$ system, wherein ^{14}C has been corrected for fractionation effects through the additional measurement of ^{13}C in each sample. Because of ^{14}C decay, there is an error introduced by this omission, but it can be shown to be small. The standard for ^{14}C is taken to be the pre-industrial atmosphere.

The ^{13}C model is similar to the ^{14}C model except that the distribution of ^{13}C relative to ^{12}C in the atmosphere, ocean, and ocean biota is controlled by fractionation factors, and fossil fuel contains ^{13}C, but not ^{14}C, in significant amount. The equilibrium fractionation between the atmosphere and oceans, which is strongly temperature dependent, is from Mook et al. (1974). The kinetic fractionation factor between the atmosphere and ocean, α_{am}, is taken to be unity (Siegenthaler and Münnich 1981). The magnitude of $\delta^{13}C$ in the pre-industrial atmosphere has been assigned the value $-6.5‰$ (Friedli et al. 1986), thus fixing the model ^{13}C standard.

Parameter adjustment

Model parameters have been adjusted to bring the tracer concentrations into about as good agreement with observation as the model dynamics and circulation field permit. The adjustment was not done in a formal way, and is probably not the very best attainable. The objective was reasonable

settings so that the general nature of the agreement could be judged.

With a given set of parameters, concentrations were set to initial values and the model "spun-up" until it reached an approximate steady state. This required about 1200 model years, 20 min on the Cray X-MP. However, model runs were ordinarily continued for 1200 more model years to insure essentially complete adjustment of concentrations.

To achieve more rapid adjustment of concentrations, the total CO_2 and alkalinity in the first two box levels were reduced by 10% and the phosphate concentration was reduced by 70%. The concentrations of ^{13}C and ^{14}C were similarly adjusted to values near expected final values. The ^{14}C source in the atmosphere was set to a value such as to resupply decaying ^{14}C in all reservoirs.

A standard case model run was made by setting the ocean average alkalinity to 2374 μ eq kg^{-1}, corresponding to a world average salinity of 34.78‰ (Takahashi et al. 1981b), and adjusting the total CO_2 to give a final atmospheric concentration near 290 ppm. The value of H in Eq. (3) was fixed at 40 μ mol kg^{-1}, and model runs were made at several values of R, which then directly controls the intensity of the new production, before settling on 20 μ mol kg^{-1}. The principle model parameters for this standard case run are summarized in Table 1. The alkalinity ended at 2373 μ eq kg^{-1}, due to loss during spin-up. The ocean average value of total CO_2, 2217 μ mol kg^{-1}, is only a little smaller than the observed value, 2254 μ mol kg^{-1} (Takahashi et al. 1981b).

The values of the parameters that prescribe remineralization of the soft-tissue flux, $DMIN(K)$, where K is the box level index, correspond to an exponential penetration depth of 700 m below the surface box (see Table 1). This value of the penetration depth was chosen to give reasonable agreement with vertical profiles, particularly the phosphate maximum. The values of the parameters that prescribe dissolution of calcium carbonate, $DISCA(K)$, were adjusted to give reasonable agreement with alkalinity profiles (see Table 1). The simplest formulation is to arrange that all the calcium carbonate dissolves on the local ocean floor. However, this produced less satisfactory agreement, particularly in the Pacific Ocean (see below).

Anthropogenic inputs

Since comparisons were to be made with GEOSECS data obtained in the 1970s, the standard case model was integrated with atmospheric CO_2 input equivalent to estimates of CO_2 from fossil fuel production and cement manufacturing (Rotty 1987). The pre-industrial model was assumed to correspond to the year 1800, estimated CO_2 yearly production was used directly after the model year 1860, and for years between 1800 and 1859 an exponential extrapolation of production between 1860 and 1900 was used. No biota source was included. The concentration of ^{13}C in fossil fuel is from Tans (1981b).

The effect of ^{14}C from nuclear explosions was simulated by forcing the atmosphere to global average yearly concentrations proposed by Tans (1981a), Table 1) for use in global carbon model intercomparisons.

Differences relative to MRH model

It was intended that this work would be a direct extension of the inorganic ocean-circulation model of Maier-Reimer and Hasselmann (1987) (MRH). However, the code for the model described here, which was run on the San Diego Supercomputer Center Cray, and the MRH code, which was run on the Hamburg Cyber 205, although once essentially identical, slowly diverged, and consequently the results cannot be directly compared. The most important differences will be listed below. Also, the circulation fields are not exactly the same although they are very similar; differences between them are due to small differences in the use of data on winds, temperature, and salinity to drive the general circulation model.

The MRH model has a meridionally diffusive atmosphere, with coefficients adjusted so that there is rapid mixing within the Northern and Southern Hemespheres and an approximately 1-year exchange time between hemispheres, rather than the uniform one-box atmosphere employed here. This difference should not have much effect because the seasonally averaged meridional atmospheric variation in CO_2 concentration is only about 5 ppm, and is mostly due to the effect of the land biota, which is not included in these models.

Ice-free ocean is specified by MRH to mean a seasonally averaged temperature greater than 0° C rather than -1.7° C used here. The ice-free area of the ocean is thus larger here by 9.4%, which is probably less realistic.

The MRH model uses an atmospheric CO_2 exchange time of approximately 11 years instead of

the 8 years used here (part of this difference is due to the difference in ice-free ocean area discussed above). The effect is sufficient to reduce ocean values of $\Delta^{14}C$ by about 16‰ relative to MRH.

The convective adjustment, instead of being done directly, is parameterized by diffusion in the MRH model. Between boxes that are to be mixed, there is introduced a diffusivity of $nL^2/\Delta t$, where n is the numer of months during which mixing occurred in the general circulation model run, Δt is a time interval equivalent to 1 year, and L is the distance between box centers. In this way, the "penetration depth" for mixing once per year is L, and this penetration depth is increased by the square root of n for more frequent mixing. The result is lower atmospheric CO_2 concentration by about 24 ppmfor the same total CO_2 concentration.

The biota new production in the MRH model is taken to be proportional to the second power of PO4 in the numerator of Eq. (3), and is larger in value by about 46%. Also, particulate organic carbon is advected as well as allowed to sink vertically.

With the same circulation field and parameter values, and the biota model disabled, the $\Delta^{14}C$ section contours essentially agree.

Comparison of model results with data

Vertical profiles

A simple way to compare model results to observation is through vertical profiles of model results and GEOSECS data averaged over broad ocean regions. Takahashi et al. (1981a), Stuiver and Östlund (1980, 1983), Stuiver et al. (1981), and Östlund and Stuiver (1980) taken together provide averages of measurements of total CO_2, alkalinity, phosphate, oxygen, and $\Delta^{14}C$ in ten ocean regions. Standard case model profiles of these species are in better agreement in the Pacific Ocean than in the Atlantic (Figs. 2-8). Phosphate is too high in both surface and deep water except in the Antarctic region; there is probably a little too

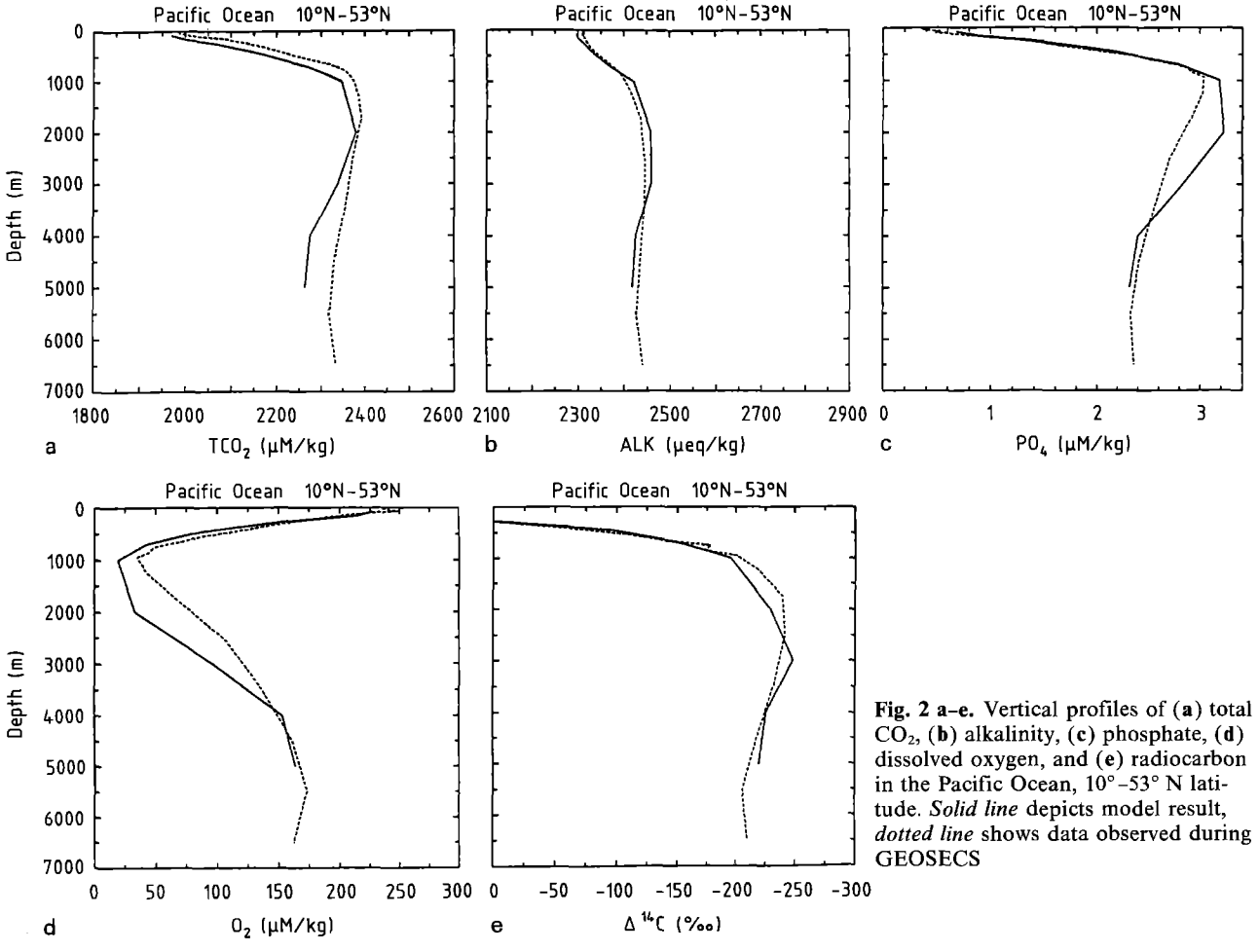

Fig. 2 a–e. Vertical profiles of (**a**) total CO_2, (**b**) alkalinity, (**c**) phosphate, (**d**) dissolved oxygen, and (**e**) radiocarbon in the Pacific Ocean, 10°–53° N latitude. *Solid line* depicts model result, *dotted line* shows data observed during GEOSECS

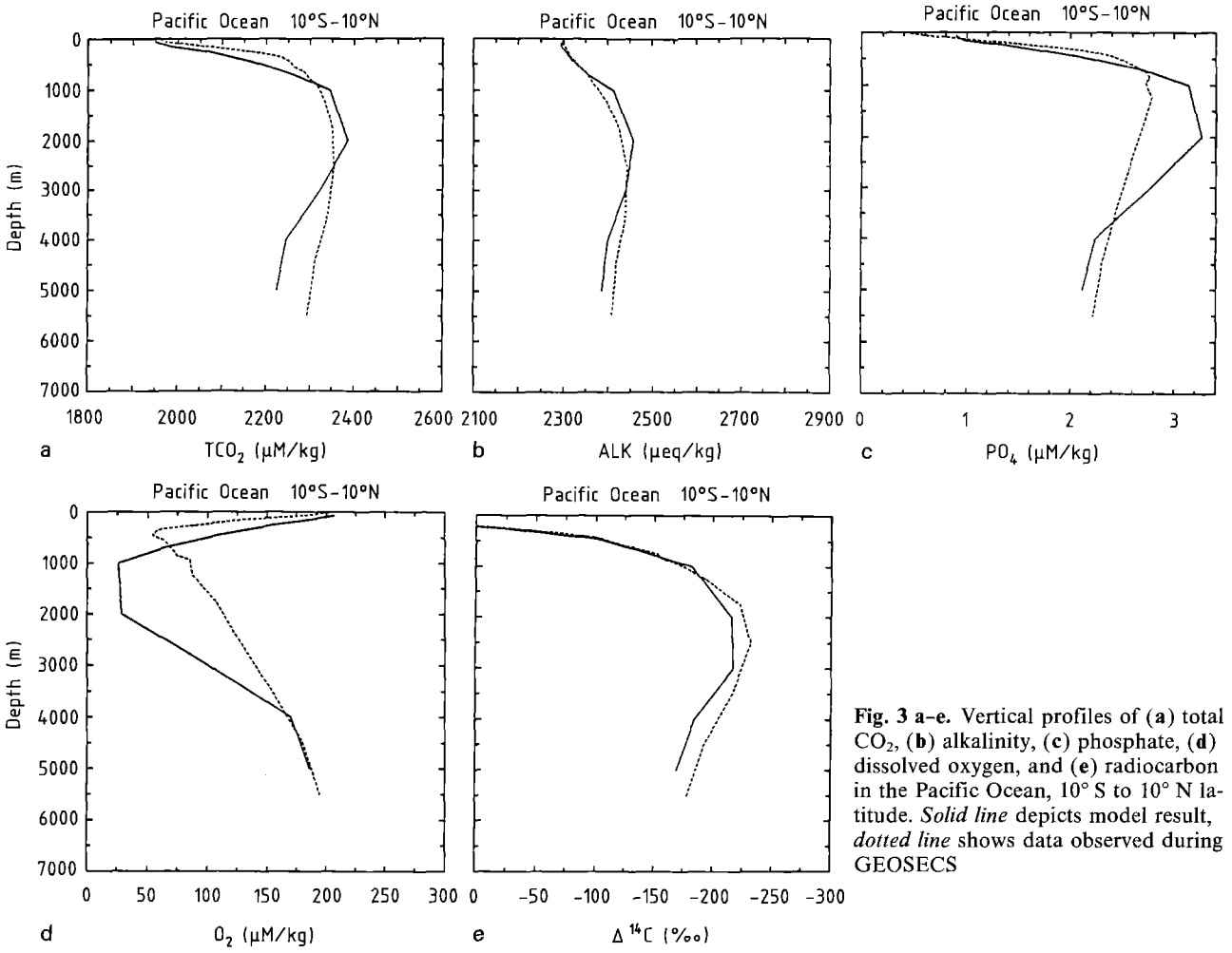

Fig. 3 a–e. Vertical profiles of (**a**) total CO_2, (**b**) alkalinity, (**c**) phosphate, (**d**) dissolved oxygen, and (**e**) radiocarbon in the Pacific Ocean, 10° S to 10° N latitude. *Solid line* depicts model result, *dotted line* shows data observed during GEOSECS

much in the model. Oxygen is too low everywhere except in the Antarctic; this implies that not enough is getting into deep water or too much is being consumed by the new production flux.

It is often difficult to know if a discrepancy between prediction and observation is due to a shortcoming of the ocean circulation field or to a shortcoming of the chemical or biota models. In this regard, the natural radiocarbon distribution is a particularly useful tracer because its fractionation corrected change relative to stable carbon, $\Delta^{14}C$, is insensitive to the formulation of the ocean biota model, as discussed below, and because it is also a measure of time constants in the system. Because ^{14}C decays, with a mean life of 8267 years, and ocean mixing is small relative to advective transport, $\Delta^{14}C$ in a water mass is a measure of the time since the water mass was last in equilibrium with the atmosphere. It should be noted, however, that contact with the atmosphere does not assure equilibrium. Indeed, the time for ^{14}C to come close to equilibrium is an order of magnitude greater than for CO_2, because the CO_2 buffer factor does not apply since ^{14}C relatively rapidly distributes throughout the several species of total carbon dioxide (bicarbonate, carbonate, dissolved CO_2). Radiocarbon from the nuclear explosions of the mid-1960s, also a very important tracer itself, is expected to have little effect on the natural ^{14}C distributions below 1000 m as measured during the GEOSECS expeditions in the 1970s, except possibly at high latitudes, and this expectation is confirmed by the model, as discussed below.

The $\Delta^{14}C$ depletion is about right in the North Pacific, insufficient in the South Pacific and Antarctic regions, and too large in the North Atlantic. This pattern is probably caused by too much deep water formation in the Antarctic region relative to the North Atlantic.

Deep water formation tends to occur episodically in sub-grid-scale sized regions in the North Atlantic Ocean during winter months as northward flowing warm water becomes more saline,

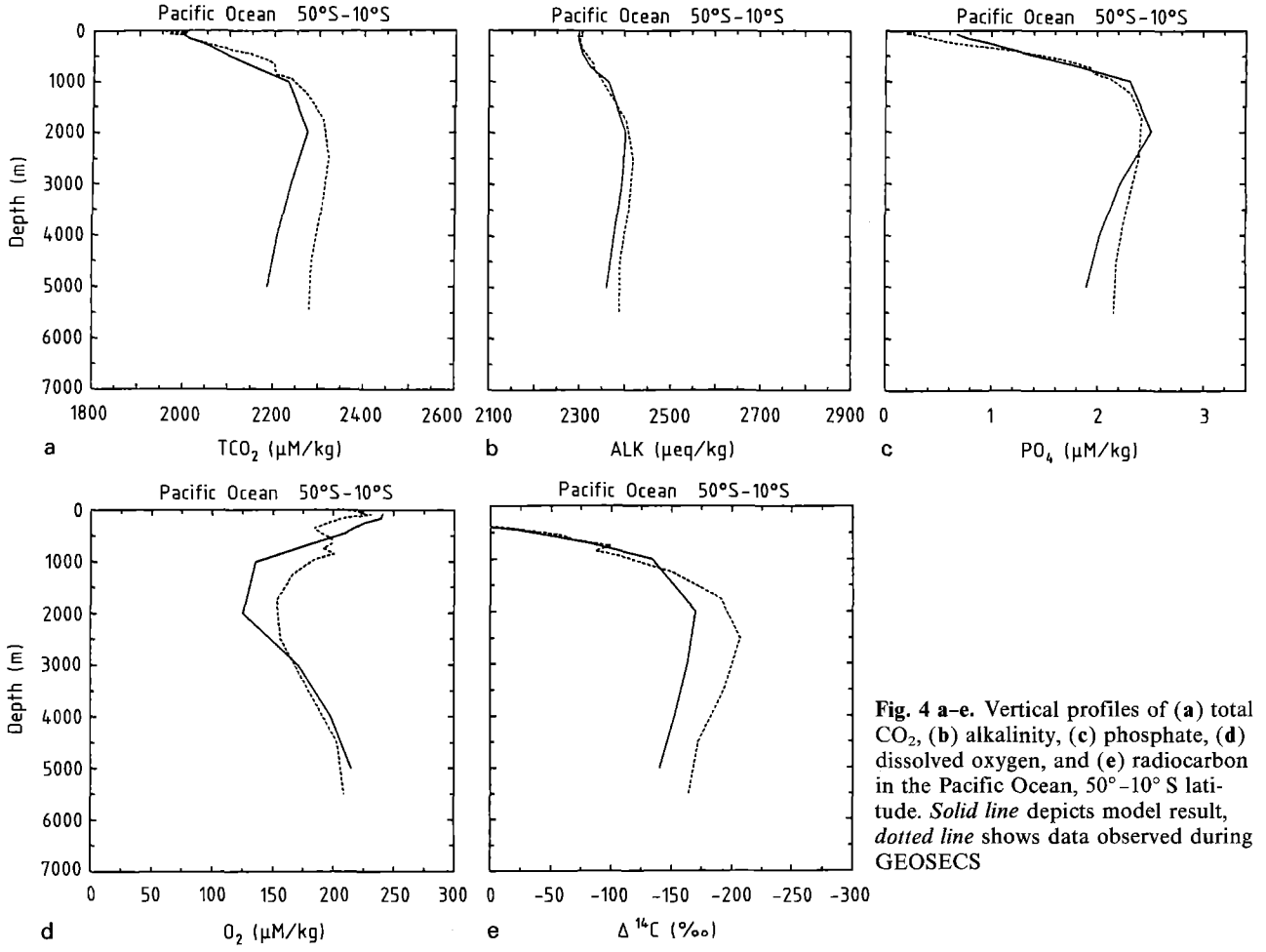

Fig. 4 a–e. Vertical profiles of (**a**) total CO_2, (**b**) alkalinity, (**c**) phosphate, (**d**) dissolved oxygen, and (**e**) radiocarbon in the Pacific Ocean, 50°–10° S latitude. *Solid line* depicts model result, *dotted line* shows data observed during GEOSECS

then cools and becomes denser than deeper water. Localized areas are found where the temperature and salinity are essentially constant from surface to ocean bottom, but at a later time the locations may be different or the phenomena may not be found at all (Clarke 1985). Figure 1 of MRH shows that convective events, as simulated by the circulation model, occur mostly in the Antarctic region, with a smaller number of events occurring in the North Atlantic. The reason for this displacement is thought to be the limited grid resolution, although the salinity increase due to ice formation is not included, and might be important to the location of deep water formation.

It was originally thought that sinking calcium carbonate could all be assumed to dissolve in boxes corresponding to the local ocean bottom. However, alkalinity profiles in the Equatorial and North Pacific regions then have a different shape than observed (Fig. 9). The model might be expected to be most sensitive to water column dissolution in these regions because the saturation horizon is shallowest there (Broecker and Peng 1982, p 75). The values of *DISCA* that have been employed (Table 1) call for dissolution of calcium carbonate to begin in the box from 850 to 1500 m, which is reasonable for the North Pacific (Chen et al. 1988), but above the saturation horizon for the Atlantic Ocean for both calcite and aragonite. It is clear that the calcium carbonate lysoclines and dissolution kinetics should be specifically modeled.

There is now good evidence for newer values of the Redfield ratios, values that associate larger changes in carbon, nitrogen, and oxygen with change in phosphate, and larger change in oxgen with change in carbon (Takahashi et al. 1985; Peng and Broecker 1987). However, use of these newer ratios,

$$C:N:P:O_2 = RC:RN:1:RO = 133:17:1:177$$

did not improve agreement between model and observations, and the larger change in oxygen re-

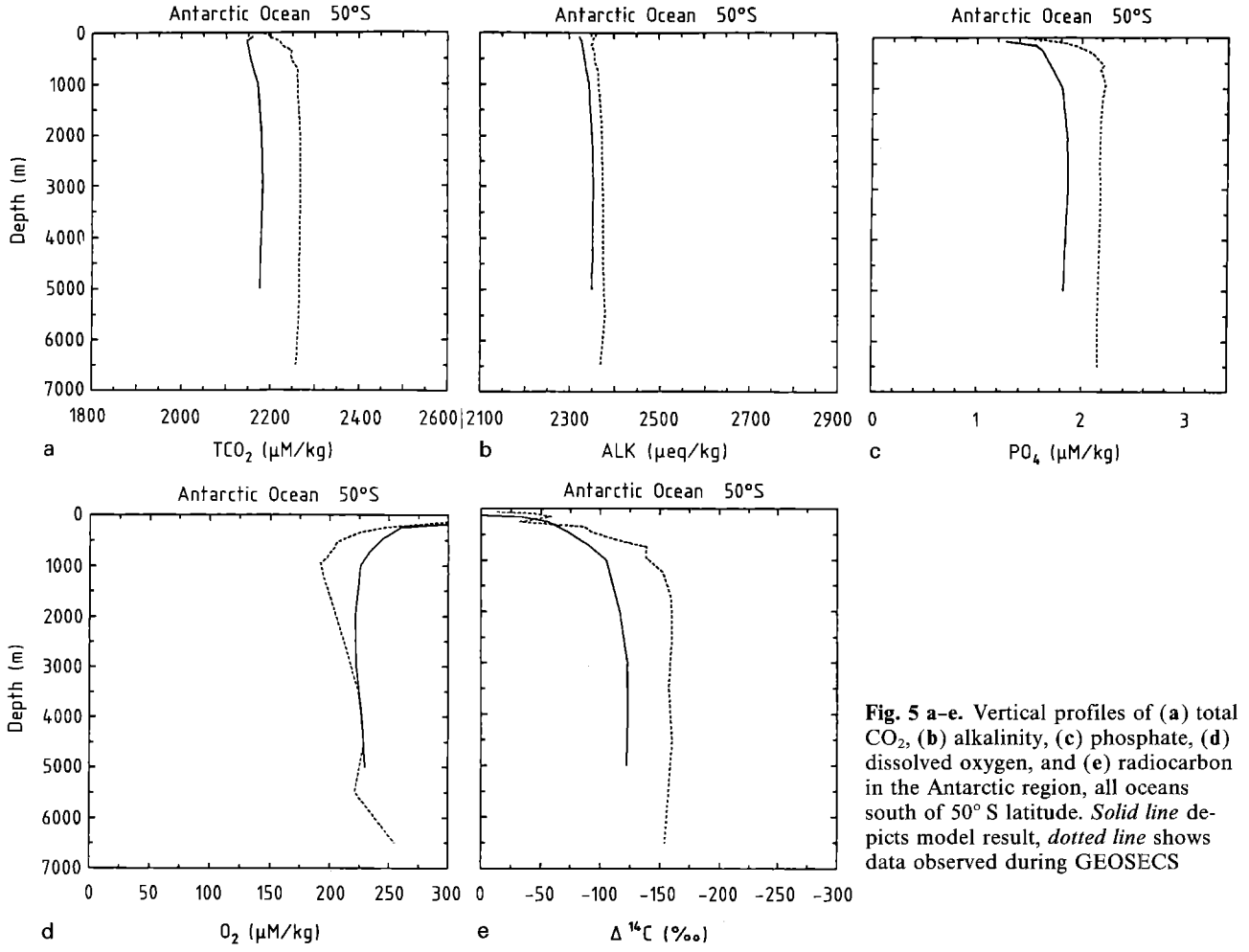

Fig. 5 a–e. Vertical profiles of (**a**) total CO_2, (**b**) alkalinity, (**c**) phosphate, (**d**) dissolved oxygen, and (**e**) radiocarbon in the Antarctic region, all oceans south of 50° S latitude. *Solid line* depicts model result, *dotted line* shows data observed during GEOSECS

lative to phosphate and carbon tends to make the oxygen depletion problem worse.

Surface distributions

Observed phosphate is very low in the surface ocean except at high latitudes and areas of strong upwelling (Reid et al. 1978). The model surface distributions, however, represent an average over the top 112.5 m. To facilitate direct comparisons, phosphate data have been averaged over the surface 112.5 m and contoured on the same grid as the model. Similar results were obtained by simply contouring 75-m values. The data are from a summary tape of world measurements (J. L. Reid, personal communication). There is variation of phosphate concentration with season, particularly near the surface in temperate and higher latitudes, and also interannual variation in the Equatorial Pacific, for example, associated with the occurrence of ENSO events every 4 years, on average. These variations have been ignored; the seasonal and interannual effects on values at 75 m and deeper, are expected to be small.

The model surface concentrations of phosphate (Fig. 10) are larger than observed by almost a factor of 2 (Fig. 11). This difference could be reduced by increasing the rate of new production by increasing the value of R in Eq. (3), but then there would be more new production than is thought to take place and vertical profiles discussed above would be less realistic. In particular, modeled oxygen would be more depleted than indicated, and it is already more depleted than observed. In more recent work, we have found that surface phosphate concentrations close to observations can be obtained by including dissolved organic carbon in the new production model (Bacastow and Maier-Reimer 1990).

Total model new production, defined as carbon sinking from the surface layer, is 4.8 gt C year^{-1}, which may be compared to the estimates of 3.4–4.7 gt C year^{-1} by Eppley and

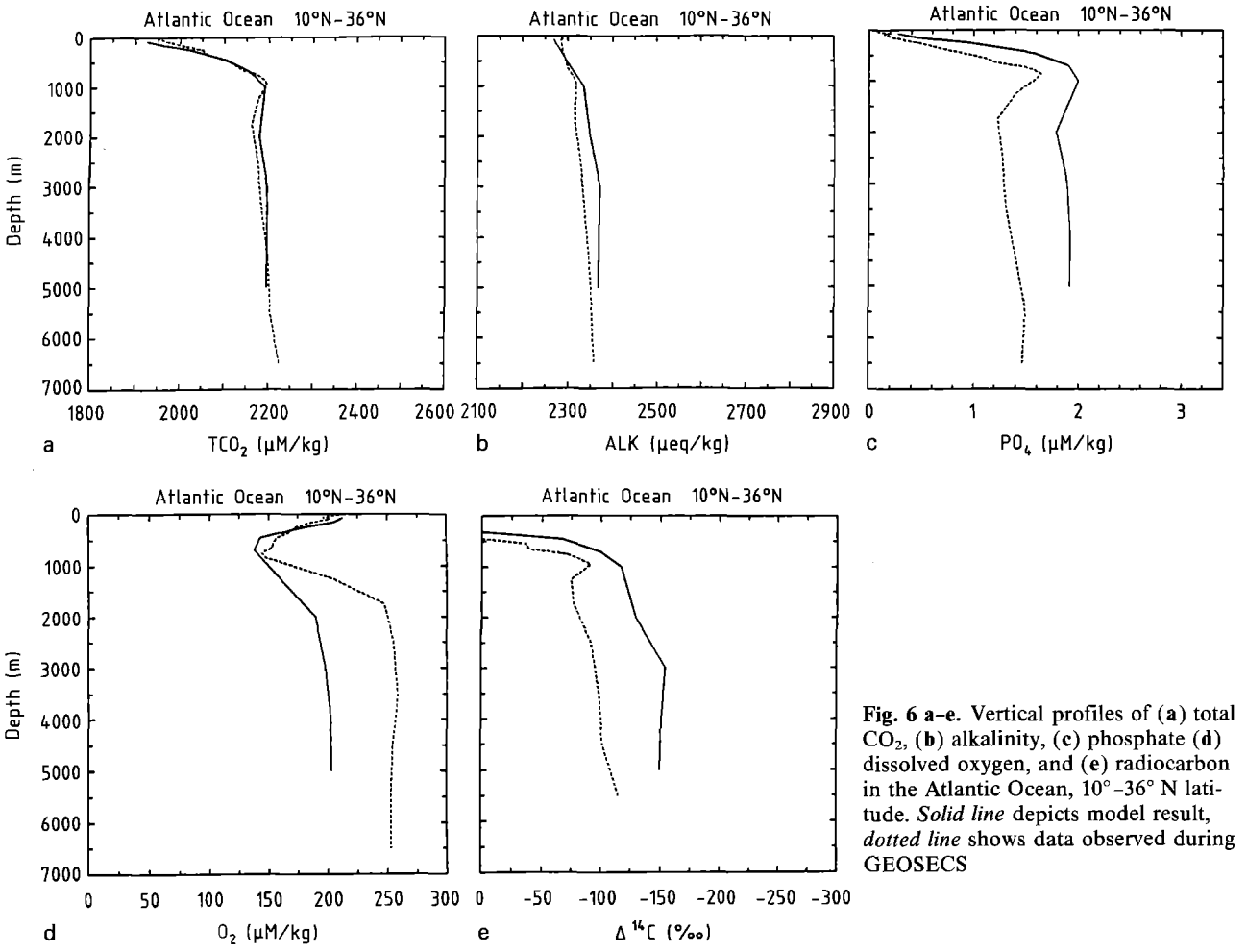

Fig. 6 a–e. Vertical profiles of (**a**) total CO_2, (**b**) alkalinity, (**c**) phosphate (**d**) dissolved oxygen, and (**e**) radiocarbon in the Atlantic Ocean, 10°–36° N latitude. *Solid line* depicts model result, *dotted line* shows data observed during GEOSECS

Peterson (1979) and 4.3 and 5.4 gt C year^{-1} by Berger et al. (1987). Recent data indicate that primary production may be much larger than indicated by the ^{14}C method, especially in the oligotrophic waters that make up large portions of the central oceanic gyres (Gieskes et al. 1979; Schulenberger and Reid 1981; Jenkins 1982). The best available map of primary production has been that of Koblentz-Mishke et al. (1970), from ^{14}C method data, but there is now much more data, and Berger et al. (1987) have produced a more detailed map (Fig. 13) from this larger data set. Also, they have estimated from sediment trap data the fraction of the primary production that is new production. The flux of soft-tissue carbon sinking below 112.5 m is estimated to be 17.8% of the primary production; the difference can be attributed to consumption and recycling within the surface ocean layer. The model predictions (Fig. 12) tend to be larger by about a factor of 2 in central ocean regions, but less near continents. Model variation between highly productive waters and oligotrophic waters is much less than observed. This small variation appears to be an artifact of the surplus of nutrient in the modeled surface waters, since the variation is much increased in models that include dissolved organic carbon and have phosphate concentrations closer to observed values, as discussed above.

The partial pressure of CO_2 exerted by ocean surface water, pCO_2, depends on total CO_2, alkalinity, and equilibrium constants which vary with temperature, and to a lesser degree, with salinity. At a given location, pCO_2 varies with season, mainly because of change in temperature and change in ocean concentrations due to biotic activity. Available data are mostly for the summertime, and are more reliable at low latitudes than high latitudes. With these qualifications, the model distribution of pCO_2 (Fig. 14) is in good agreement with observation (Fig. 15). The model pCO_2 shows a strong high in the Equatorial Pacific, a high in the Equatorial Atlantic off the coast of Africa, and lows at high latitudes. Lower

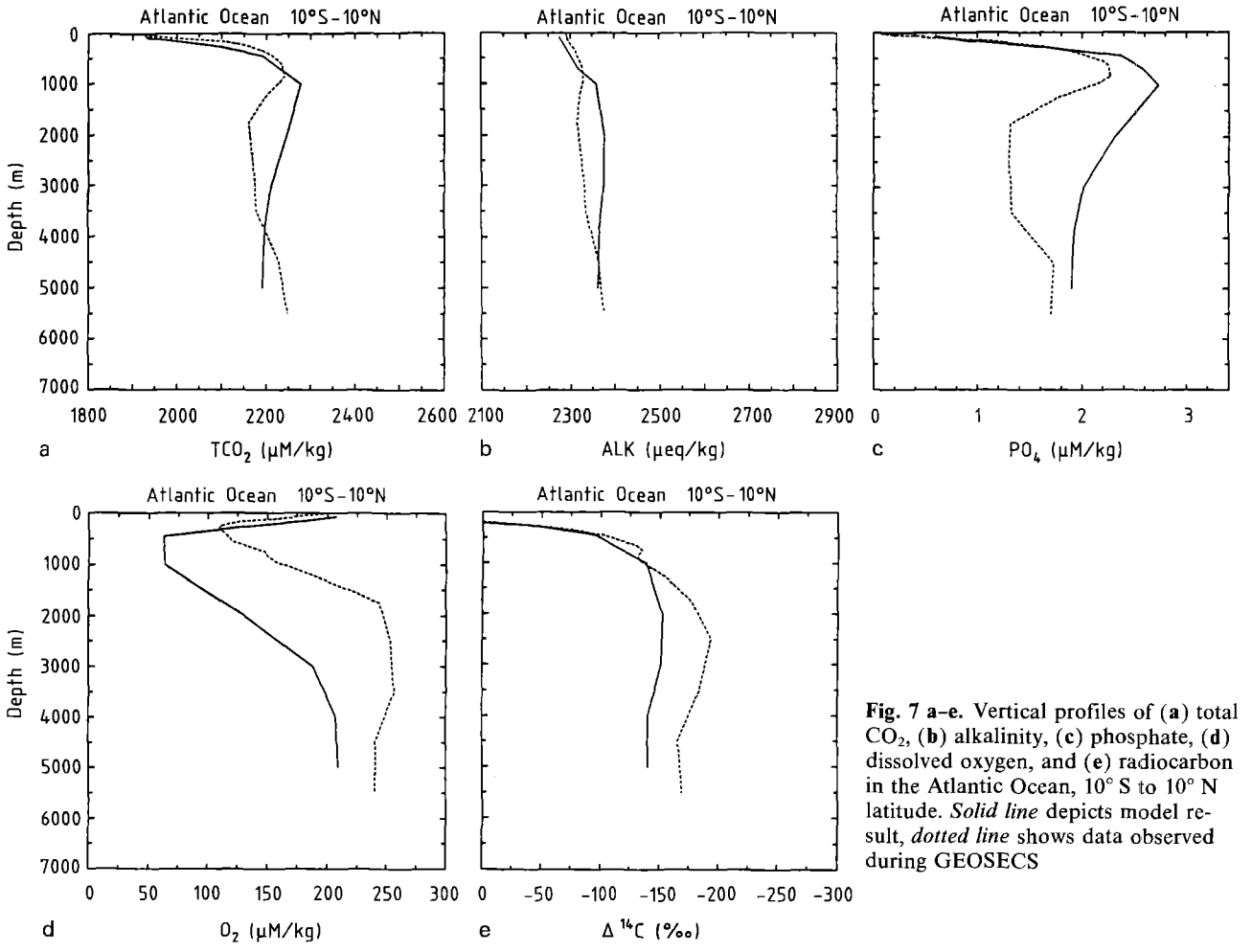

Fig. 7 a–e. Vertical profiles of (**a**) total CO_2, (**b**) alkalinity, (**c**) phosphate, (**d**) dissolved oxygen, and (**e**) radiocarbon in the Atlantic Ocean, 10° S to 10° N latitude. *Solid line* depicts model result, *dotted line* shows data observed during GEOSECS

values are seen in the Western Pacific and Western Atlantic than further east, as the gyre surface flow carries warm, outgassing water northward where it rapidly cools. These structures are all seen in data on pCO_2 in surface ocean water (Keeling 1968; Takahashi et al. 1983).

Keeling et al. (1989) have adjusted surface sources and sinks in a three-dimensional atmospheric model to agree with observed atmospheric CO_2 data. They estimate that the surface ocean to atmosphere flux of carbon in the global equatorial region ($\pm 15.65°$ of the Equator) is approximately 2.0 gt C year^{-1}. The ocean model predicts 1.8 gt C year^{-1}.

The question of the cause of the observed patterns of source (positive values in Figs. 14 and 15) and sink (negative values) for atmospheric CO_2 is interesting. It has been discussed extensively by Brewer (1986). The main determinants are the ocean surface temperature and the effect of the ocean biota. Recently, Volk and Liu (1988) have examined the question with a series of box models. They argue that the dominant cause of the source/sink distribution is ocean surface temperature. A comparison of the (pre-industrial) ocean–atmosphere pCO_2 distributions with and without ocean biota (Fig. 16) tends to support the arguments of Volk and Liu. The patterns of source and sink are very nearly the same with and without an ocean biota.

The model surface distribution of total CO_2 (Fig. 17) shows a Pacific Equatorial peak presumably due to upwelling, lower values in the central gyres, and higher values at high latitudes, probably due to transport through the atmosphere from the warmer waters to the colder waters (as indicated by pCO_2 surface pressures relative to the atmosphere). The surface alkalinity distribution (Fig. 18) is much more nearly constant than that of total CO_2.

The surface pre-industrial distribution of $\Delta^{14}C$ (Fig. 19) shows higher values in gyre areas where Ekman pumping produces downwelling than in areas where upwelling brings to the surface water

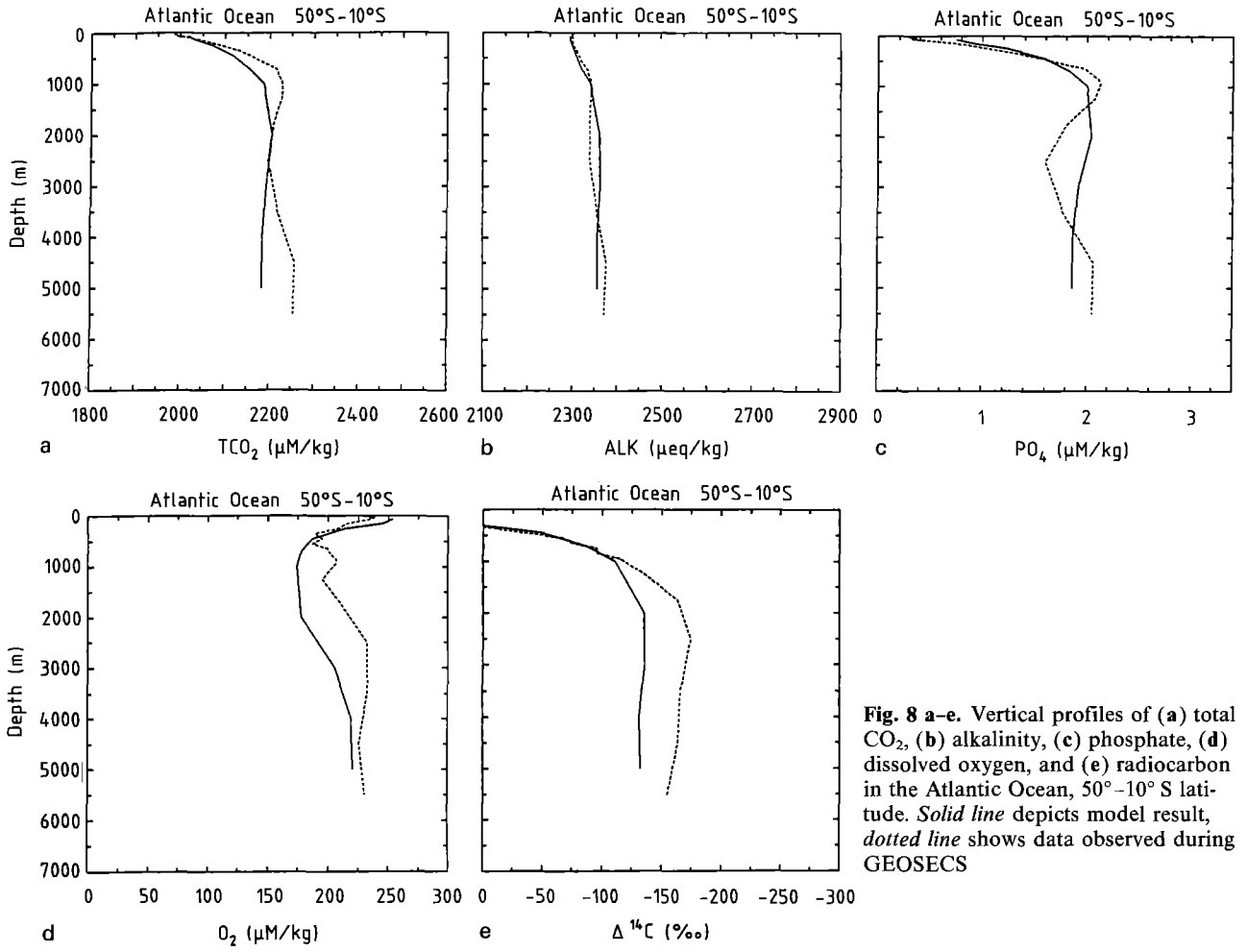

Fig. 8 a–e. Vertical profiles of (**a**) total CO_2, (**b**) alkalinity, (**c**) phosphate, (**d**) dissolved oxygen, and (**e**) radiocarbon in the Atlantic Ocean, 50°–10° S latitude. *Solid line* depicts model result, *dotted line* shows data observed during GEOSECS

more depleted in ^{14}C. This difference is observed in radiocarbon measurements in banded corals (Druffel and Suess 1983, Fig. 29 p 1272).

The surface values of $\delta^{13}C$ (for the year 1975) are lower than data given by Kroopnick et al. (1977, p 304), but show some similarities of structure (Fig. 20). They agree better with the levels indicated in section plots in the Atlantic and Pacific (Kroopnick 1985).

Uptake of bomb radiocarbon by the surface ocean

Druffel and Suess (1983) have also found that the ocean response to bomb ^{14}C was much larger in ocean regions characterized by downwelling (Bermuda) than in regions where there is strong upwelling (Galapagos Islands). The model also shows this behavior (Fig. 21).

Vertical sections

Vertical profiles, as in Figs. 2–9, are useful in comparing model predictions to data because differences stand out, but a more demanding comparison can be made by comparing contours in the vertical sections measured during the GEOSECS expeditions. Two north-south sections were measured in each of the three oceans, and sections have been published in atlases (A. E. Bainbridge, undated; Craig et al. 1981; Spenser et al. 1982). However, comparisons are easiest to make if both predictions and observations are plotted on the same scale. In the GEOSECS Atlases, the latitudinal sections are not linear in the latitude, but instead are linear in the distance between stations, which were not all at the same longitude.

We have recontoured GEOSECS data (obtained from Physical & Chemical Oceanographic Data Facility, Scripps Institution of Oceanography, La Jolla, California 92093) projected on a linear latitudinal scale. The contoured data is uncorrected, and accepted, unless marked as a known error, without review for consistency. The

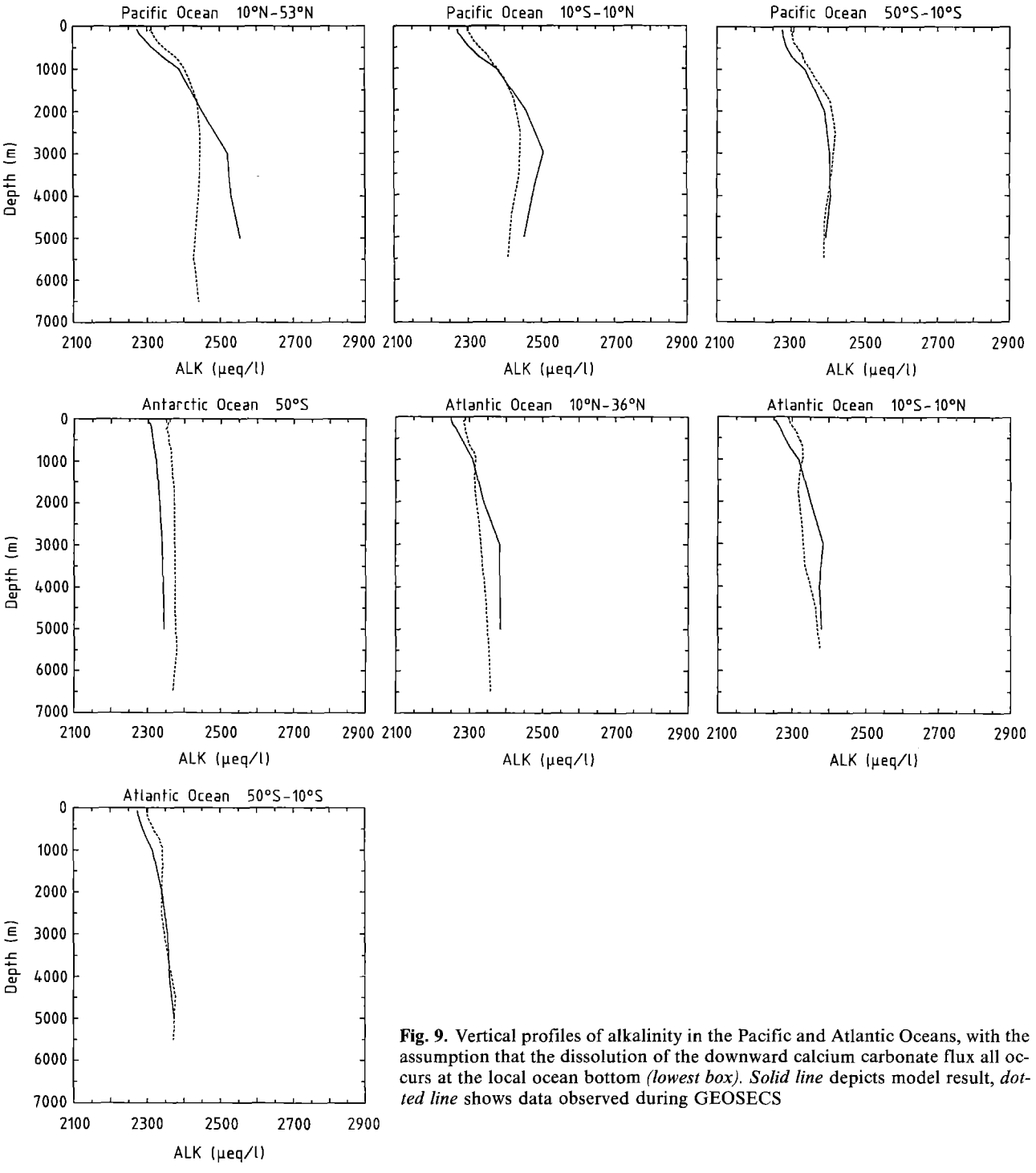

Fig. 9. Vertical profiles of alkalinity in the Pacific and Atlantic Oceans, with the assumption that the dissolution of the downward calcium carbonate flux all occurs at the local ocean bottom *(lowest box)*. *Solid line* depicts model result, *dotted line* shows data observed during GEOSECS

model predictions used for comparison, are obtained from the vertical stacks of grid points closest to the GEOSECS track.

The general shape of the model contours is similar to that observed (Figs. 22–33). All the contours, however, show the effect of too much deep water formation in the southern oceans relative to the North Atlantic. This is probably most clearly seen in the $\Delta^{14}C$ comparisons.

$\Delta^{14}C$ in the Atlantic. The data show that radiocarbon in the deep water of the equatorial and mid-latitude Atlantic Ocean is depleted relative to standard by about 100‰ and the depletion in-

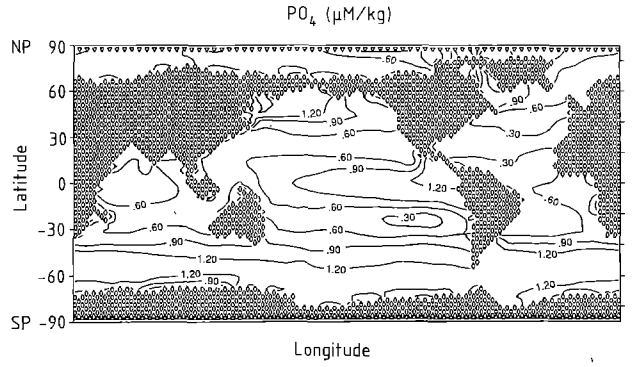

Fig. 10. Model distribution of inorganic phosphate (μ mol kg^{-1}) in the surface ocean layer (112.5 m thick)

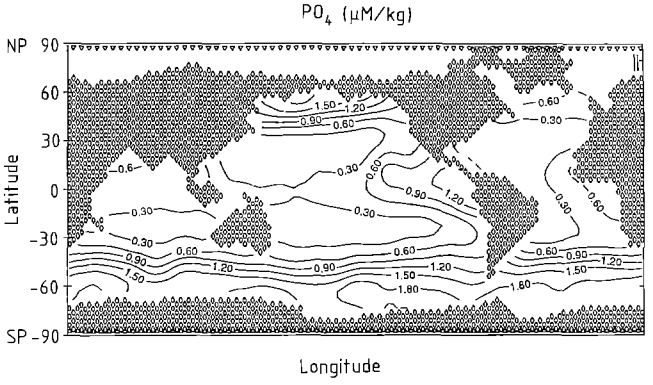

Fig. 11. Observed distribution of inorganic phosphate (μ mol kg^{-1}), averaged over the surface 112.5 m depth so as to correspond to the model

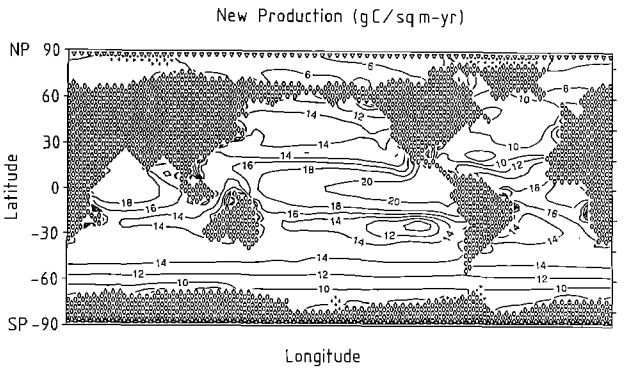

Fig. 12. Model distribution of new production (g m^{-2} $year^{-1}$) in the ocean. The *small diamonds* which make up the continents surround each (dry) scalar point, and thereby indicate the resolution of the model. The *small pluses* indicate ice-covered water

creases to 140‰ to the south (Fig. 22). The model shows a depletion of 140‰ in the midlatitudes but decreases to 100‰ to the south, just the opposite of the observations. The decrease is probably caused by too much convection in the modeled southern oceans. The data also show a strong downward slope to contours of −40‰, −60‰, and −80‰ at high northern latitudes, undoubtedly caused by deep water formation. The model shows downward slope to these contours, but the slope is much smaller than observed.

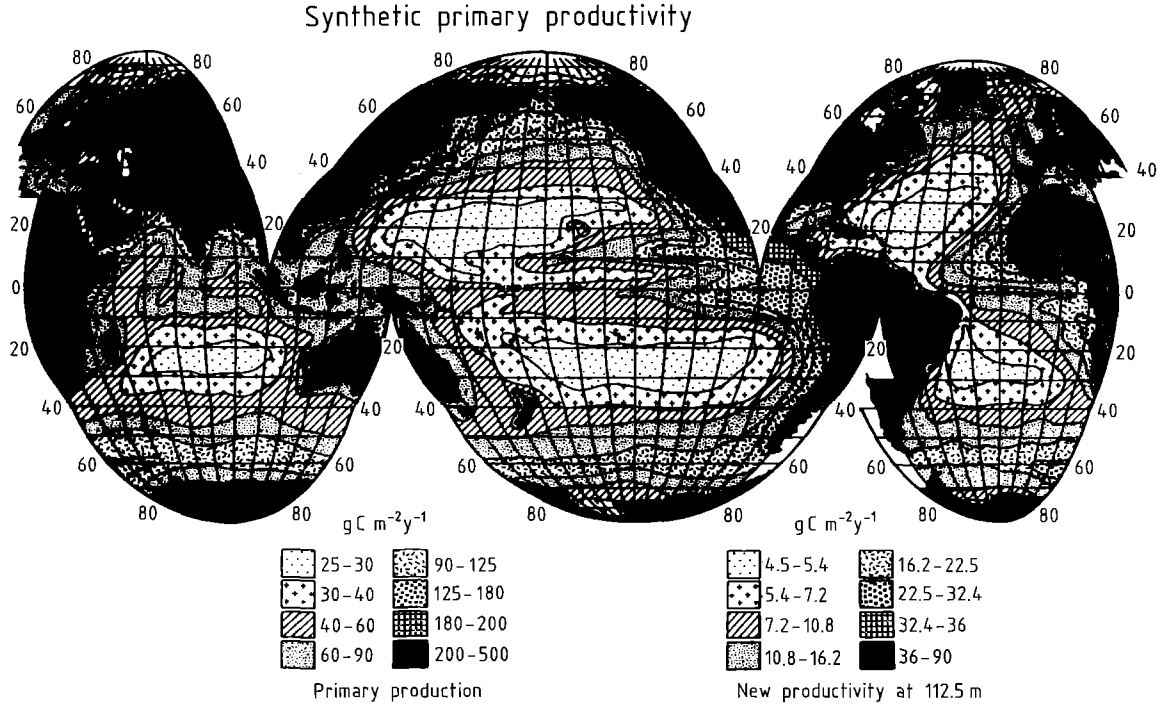

Fig. 13. Distribution of ocean primary productivity according to Berger et al. (1987). New productivity passing through the depth of the model surface layer is estimated to be 17.8% of the primary productivity (see key to right above)

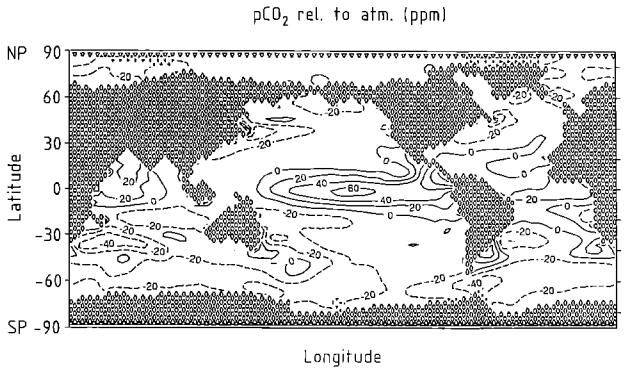

Fig. 14. Model distribution of ΔpCO_2 (ppm) in the surface ocean. ΔpCO_2 is the partial pressure of CO_2 exerted by the ocean surface less the partial pressure in the atmosphere. Contours of negative value are *dashed*

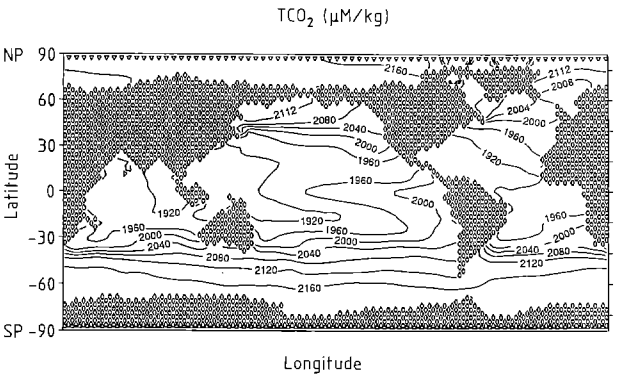

Fig. 17. Model distribution of inorganic total CO_2 (μ mol kg^{-1}) in the ocean surface layer (112.5 m thick)

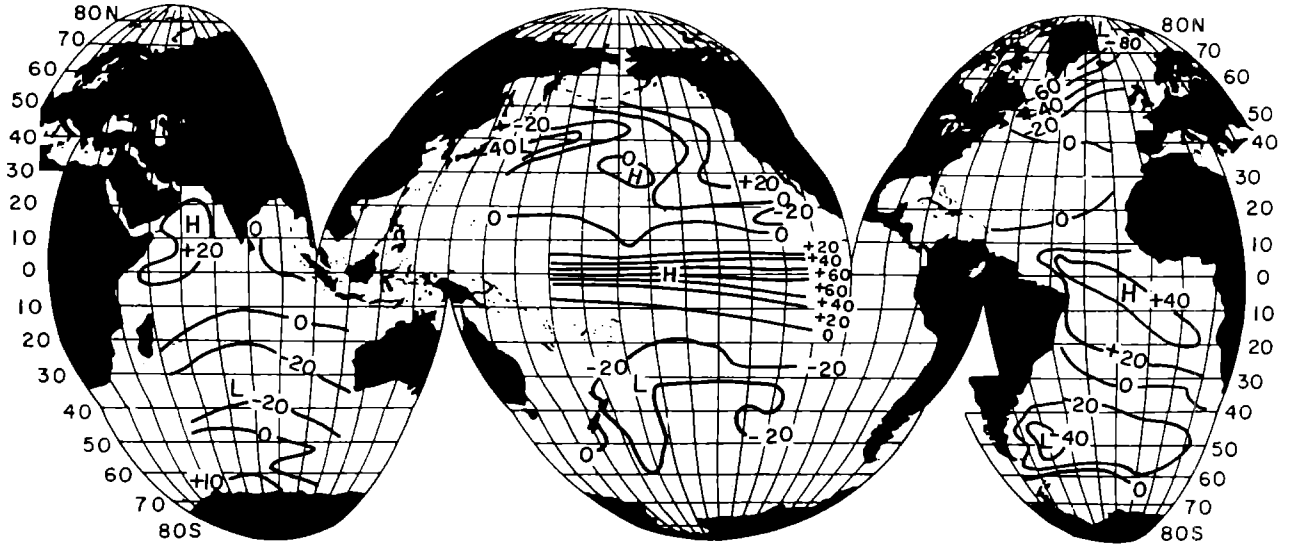

Fig. 15. Observed distribution of ΔpCO_2 (ppm) in the surface ocean (Takahashi et al. 1983)

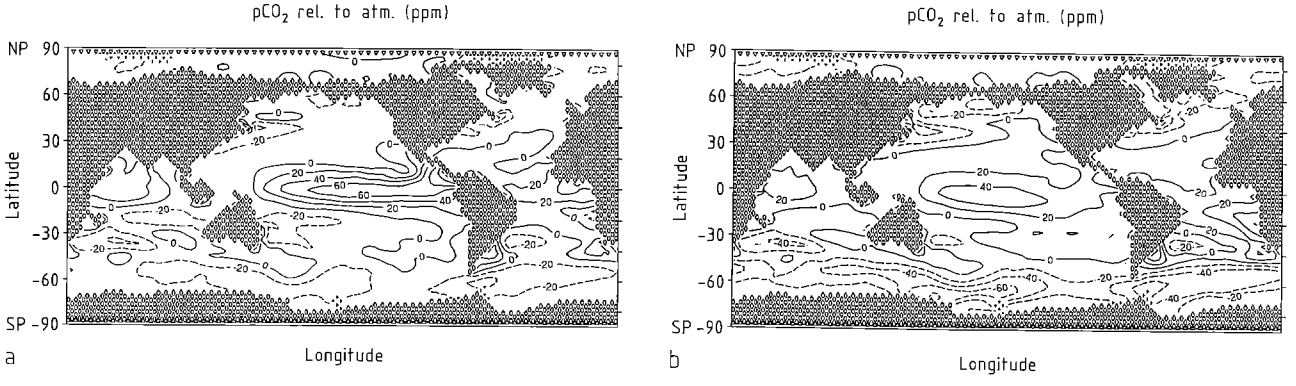

Fig. 16a, b. Comparison of (pre-industrial) ΔpCO_2 (ppm) in the surface ocean: **a** with ocean biota, and **b** without ocean biota

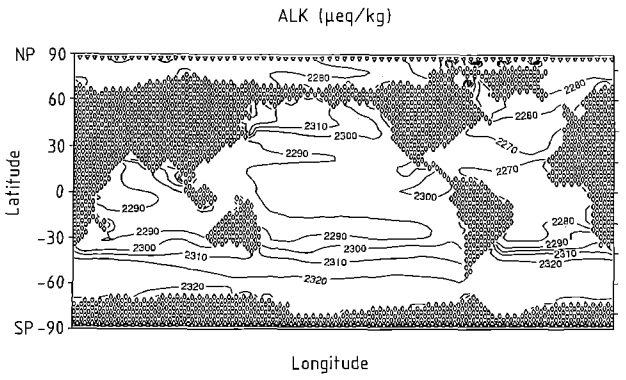

Fig. 18. Model distribution of titration alkalinity (μ eq kg^{-1}) in the ocean surface layer

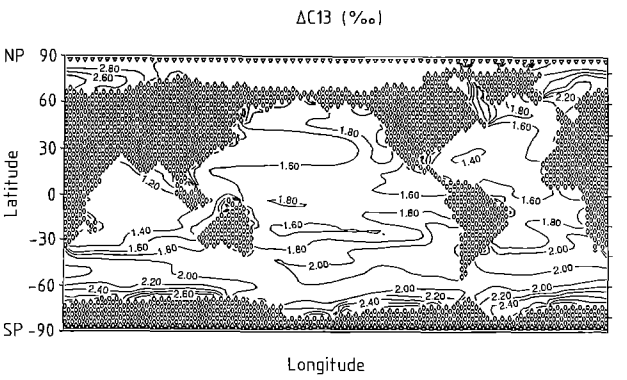

Fig. 20. Model distribution of δ^{13}C (‰) in the ocean surface layer

$\Delta^{14}C$ in the Pacific. In the Pacific, the data (Fig. 23) show evidence for deep water formation in the South Pacific from water already depleted in ^{14}C in the downward thrust of the -160‰ contour and the curving under of the -180‰, -200‰, and -220‰ contours, implying a flow of "younger" water under a central core of "older" water. The model shows a strong downward slope to the -120‰ contour not seen in the data. Also, the water in the Antarctic region is less depleted in the model than shown by the data. The model contour at -140‰ is located very close to the -180‰ contour of the data.

Phosphate. In both the Atlantic (Fig. 24) and the Pacific (Fig. 25), the phosphate maxima under the equatorial zone is too intense and too deep. A more shallow remineralization of the new production flux, by readjustment of the values of *DMIN* (Table 1), would raise the phosphate maxima, but at the same time would be expected to raise phosphate concentrations in the surface ocean, which are already too high. One also sees evidence, similar to that discussed above for Δ^{14}C, that there is not enough deep water formation in the North At-

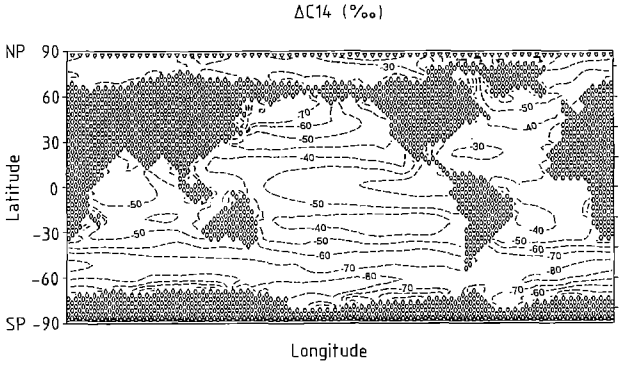

Fig. 19. Model distribution of pre-industrial Δ^{14}C (‰) in the ocean surface layer

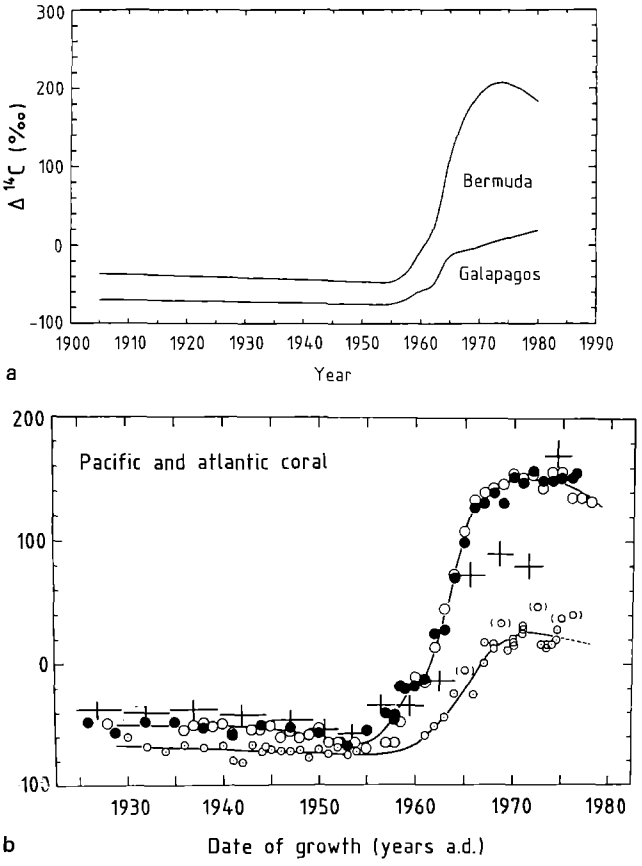

Fig. 21a, b. Response of the ocean surface water to atmospheric bomb ^{14}C: **a** model at Bermuda and the Galapagos Islands; **b** observations of ^{14}C in banded corals at Bermuda, Florida, and Belize, and the Galapagos Islands. ● Belize (Drufel 1980a); ○ Florida (Druffel and Linick 1978); ⊙ Galapagos (Druffel 1981); + Bermuda (Nozaki et al. 1978). From Druffel and Suess (1983)

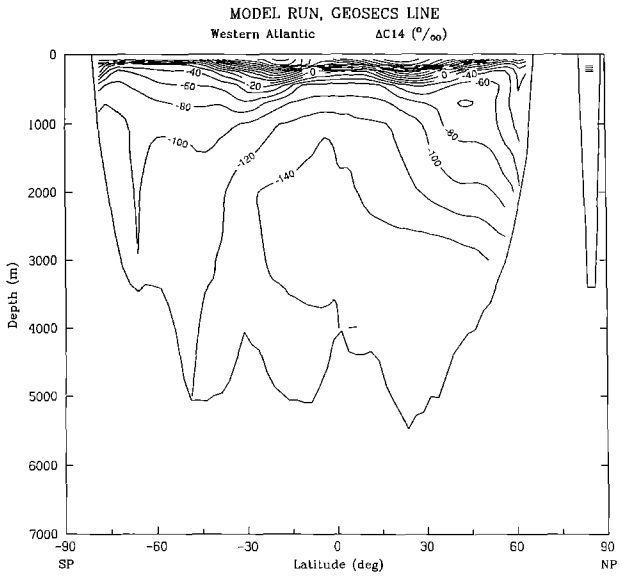

a

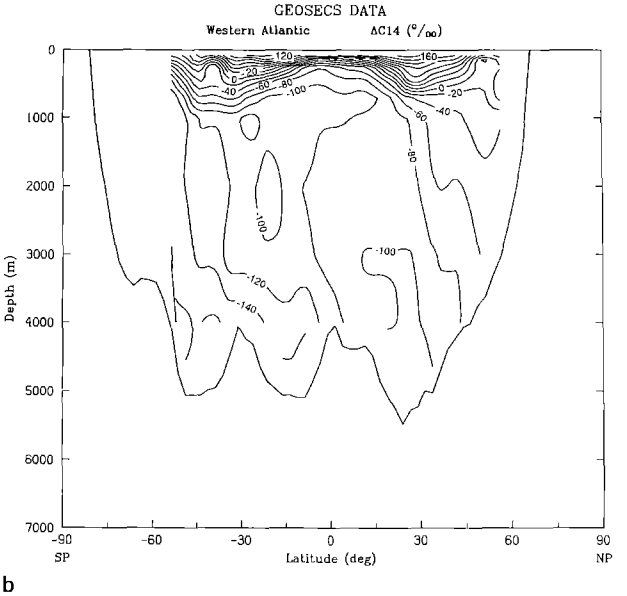

b

Fig. 22 a, b. Vertical sections of $\Delta^{14}C$ (‰) in Western Atlantic Ocean: **a** model; **b** GEOSECS data

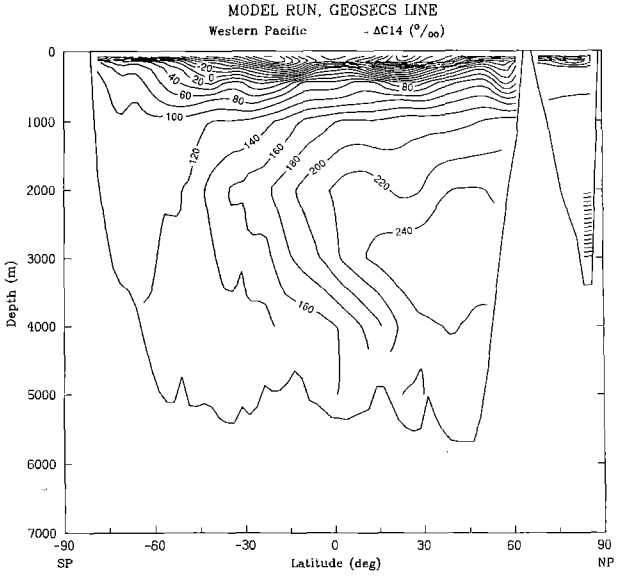

a

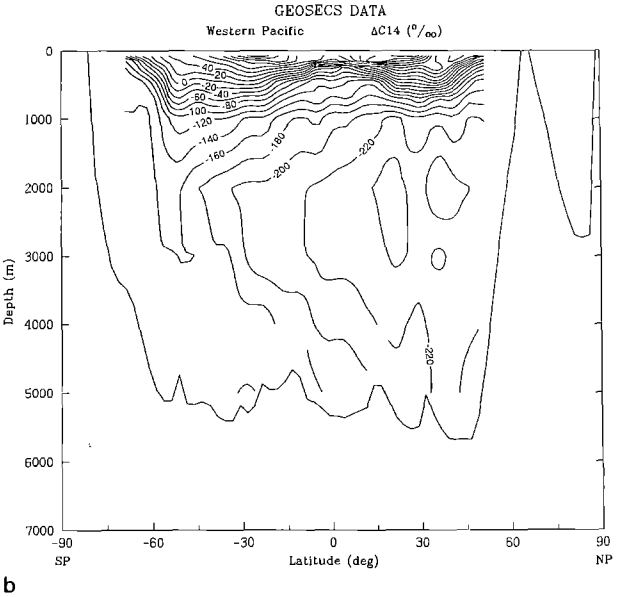

b

Fig. 23 a, b. Vertical sections of $\Delta^{14}C$ (‰) in Western Pacific Ocean: **a** model; **b** GEOSECS data

lantic and too much in the southern oceans. The 1.20 and 1.50 μ mol kg^{-1} contours in the North Atlantic data are much shallower in the model; the 2.10 μ mol kg^{-1} contour in the South Pacific data is much deeper in the model.

Oxygen. Dissolved oxygen consumption is a measure of remineralization of organic material. In both the Atlantic (Fig. 26) and the Pacific (Fig. 27), the minimum is too deep and too intense. Both oceans are too low in oxygen, probably because of a lack of deep water formation in the North Atlantic where the surface dissolved oxygen concentration is high. The horizontal structure of the contours of 220, 240, 260, and 280 μ mol kg^{-1} in the model North Atlantic contrast with the predominantly vertical structure in the data.

Total carbon dioxide. The model total CO_2 maximum under the equatorial high productivity regions is a little too deep, in comparison to obser-

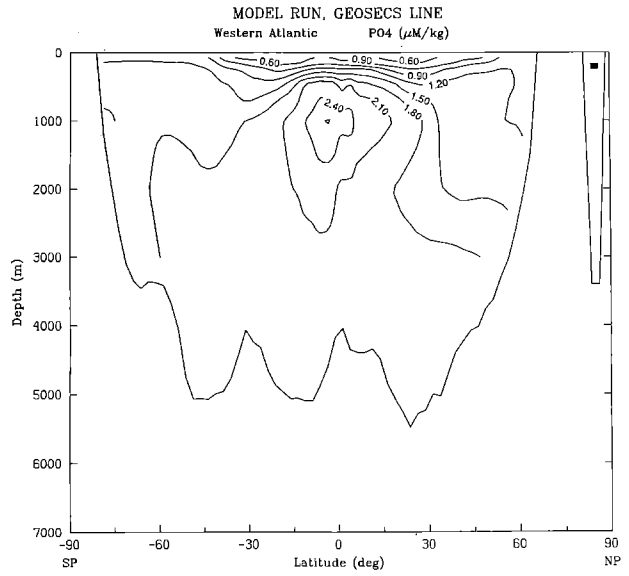

a

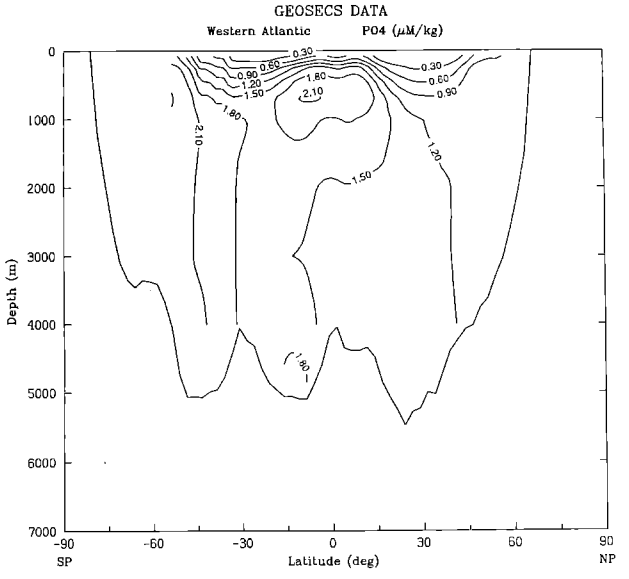

b

Fig. 24a, b. Vertical secitons of inorganic phosphate (μ mol kg^{-1}) in Western Atlantic Ocean: **a** model; **b** GEOSECS data

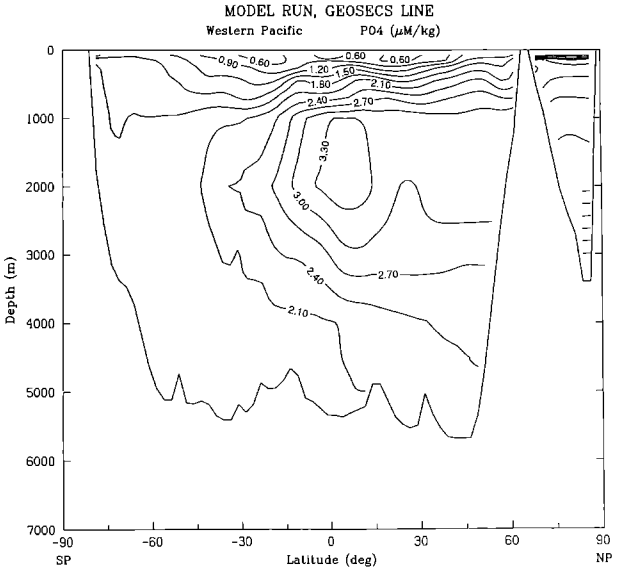

a

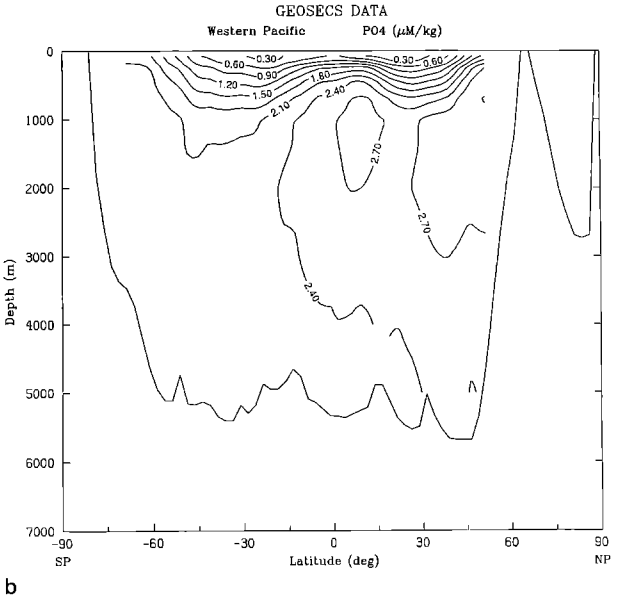

b

Fig. 25a, b. Vertical sections of inorganic phosphate (μ mol kg^{-1}) in Western Pacific Ocean: **a** model; **b** GEOSECS data

vation (Figs. 28 and 29). The data and the model contours show a shallowing in the equatorial regions, presumably due to upwelling, and a shallowing at high latitudes, probably caused by uptake from the atmosphere of CO_2 in these regions of colder water.

Alkalinity. The model alkalinity maximum under the equatorial high productivity regions is too large in both the Atlantic (Fig. 30) and Pacific (Fig. 31). In these regions of high surface nutrient, the dominant phytoplankton tend to be diatoms, which fix silica and consequently do not cause alkalinity to be transported. The chemical model should also include dissolved silica, and the biota model should distinguish between organisms which precipitate calcium carbonate and organisms which precipitate silica.

$\delta^{13}C$. The GEOSECS data for $\delta^{13}C$ could not be

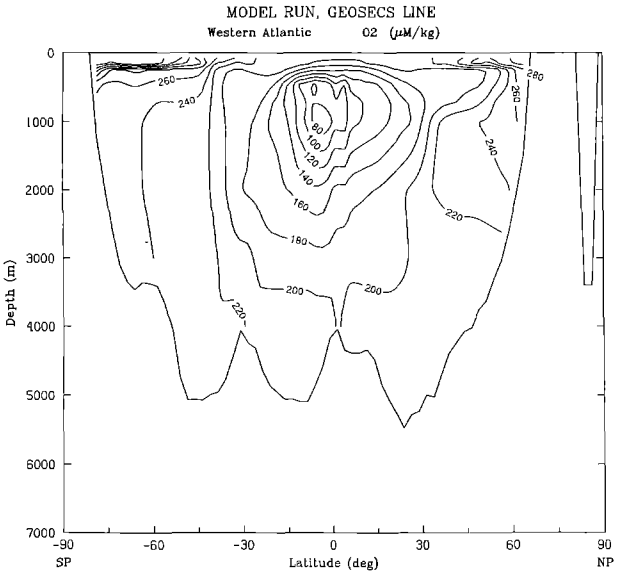

a

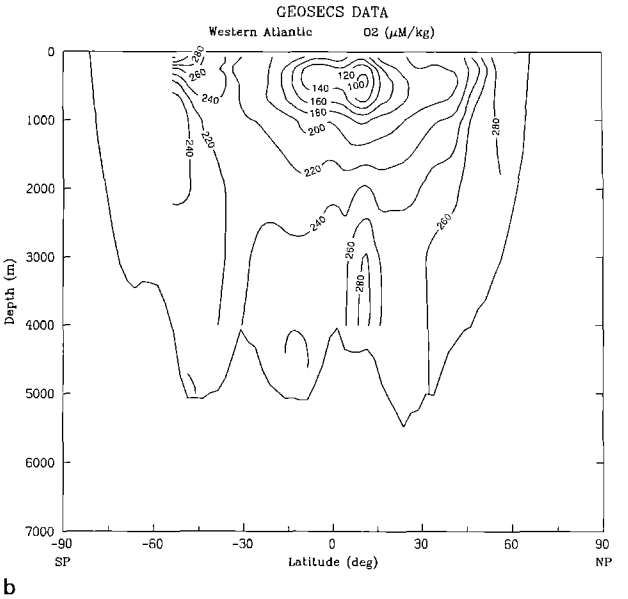

b

Fig. 26a, b. Vertical sections of dissolved oxygen (μ mol kg^{-1}) in Western Atlantic Ocean: **a** model; **b** GEOSECS data

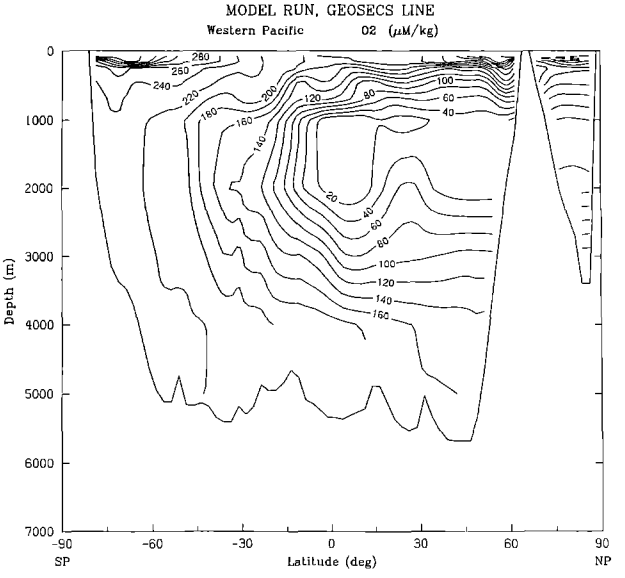

a

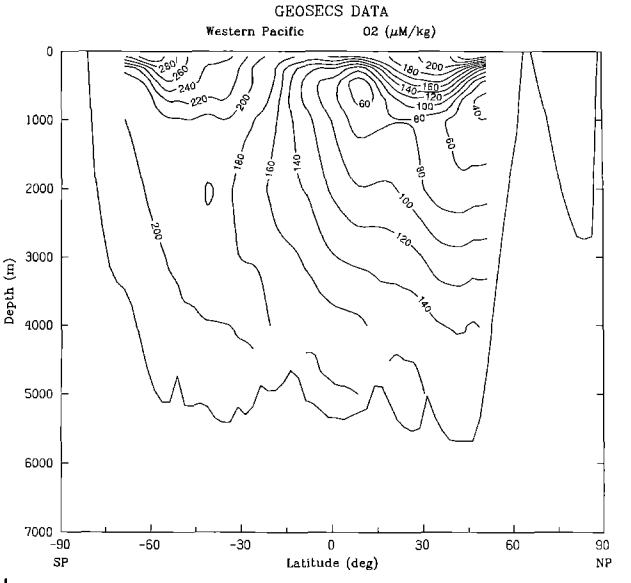

b

Fig. 27a, b. Vertical sections of dissolved oxygen (μ mol kg^{-1}) in Western Pacific Ocean: **a** model; **b** GEOSECS data

easily recontoured on our scale because the corrections were too numerous and important (Kroopnick 1985). However, Kroopnick (1985) has published contours on a linear latitudinal scale that is very similar to our scale. Surface values in the model Atlantic section (Fig. 32) and the Pacific section (Fig. 33) agree well with observations, but deeper values in both oceans tend to be about 1‰ too large. The reason for this large difference is not known.

Fossil fuel uptake

By introducing into the model atmosphere CO_2 from historical records of fossil fuel and cement production, we calculate the ocean-borne fraction of the model with no land biota. For the standard case model the ocean-borne fraction for recent time (1955–1975) is 0.32, compared to 0.34 for the box-diffusion model calibrated by natural ^{14}C and 0.40 for the box-diffusion model calibrated

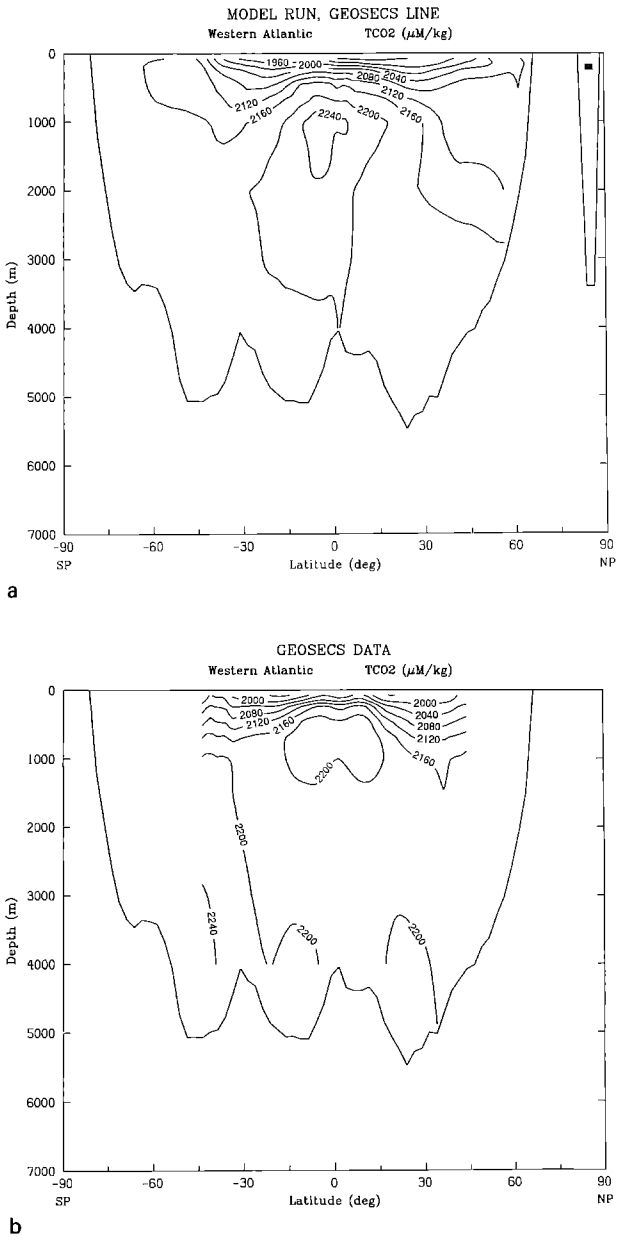

Fig. 28a, b. Vertical sections of total CO_2 (μ mol kg^{-1}) in Western Atlantic Ocean: **a** model; **b** GEOSECS data

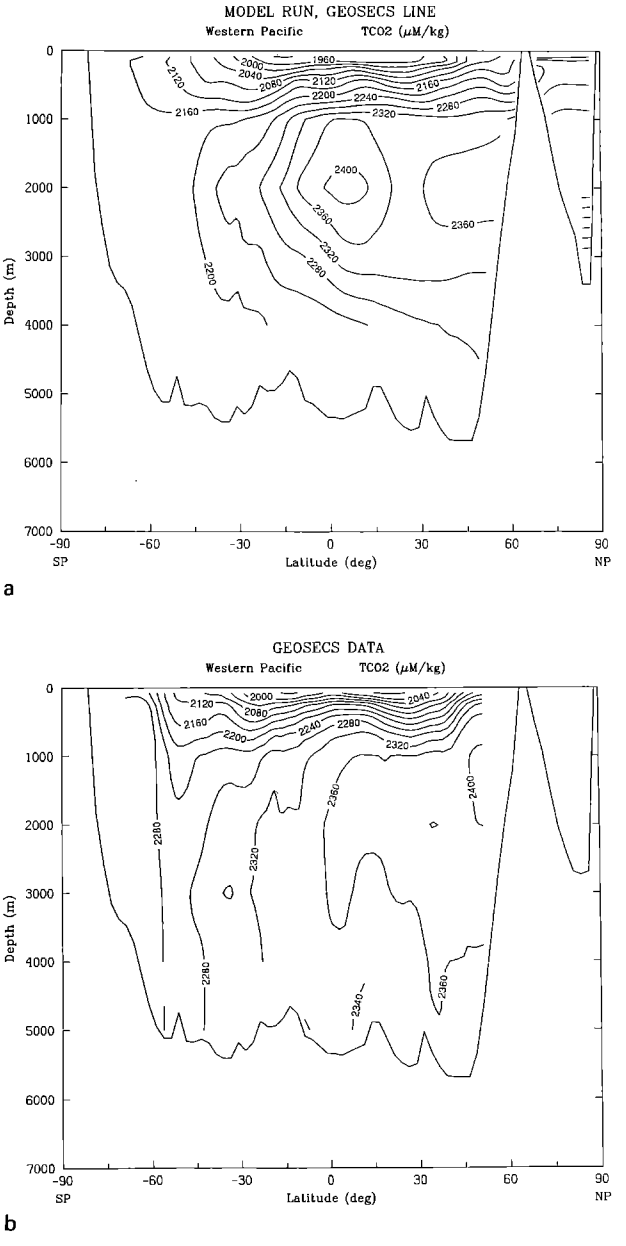

Fig. 29a, b. Vertical sections of total CO_2 (μ mol kg^{-1}) in Western Pacific Ocean: **a** model; **b** GEOSECS data

by bomb ^{14}C [with parameters essentially as given by Siegenthaler (1983)]. Other versions of the circulation field, derived from different wind, temperature, and salinity forcing of the general circulation model, resulted in ocean-borne fractions of 0.30 and 0.29.

As MRH have pointed out, there are really no adjustable parameters for calculating the uptake of fossil fuel, since the ocean biota do not play a direct role in this uptake and serve only to set the surface total CO_2 concentration and alkalinity for a given amount of CO_2 in the system, and we tune this total amount to give an atmospheric concentration near the known pre-industrial value. Nevertheless, there is some uncertainty due to the modeling of convective mixing in a seasonally averaged model. The uptake of fossil fuel is particularly sensitive to convectice mixing. The values of the ocean-borne fraction given above are for convective mixing done directly once per year for those boxes that are convectively mixed one or more times during a year by the circulation mod-

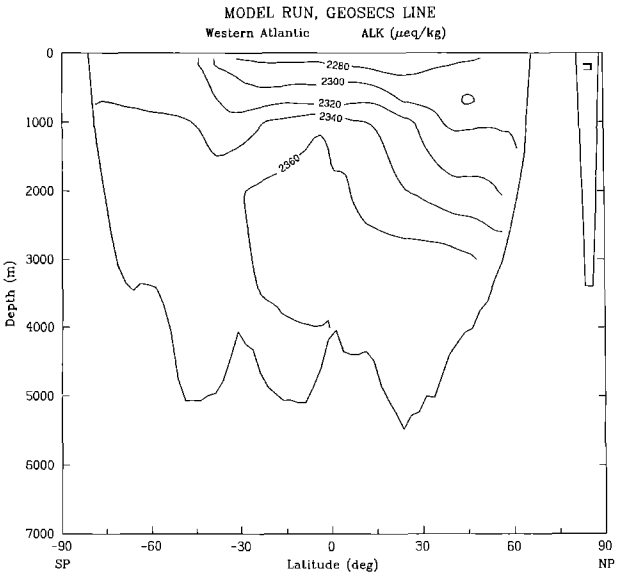

a

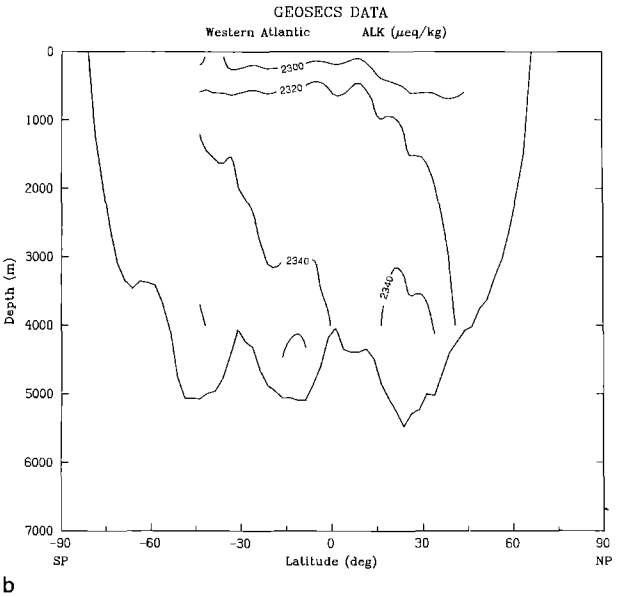

b

Fig. 30 a, b. Vertical sections of titration alkalinity (μ eq kg^{-1}) in Western Atlantic Ocean: **a** model; **b** GEOSECS data

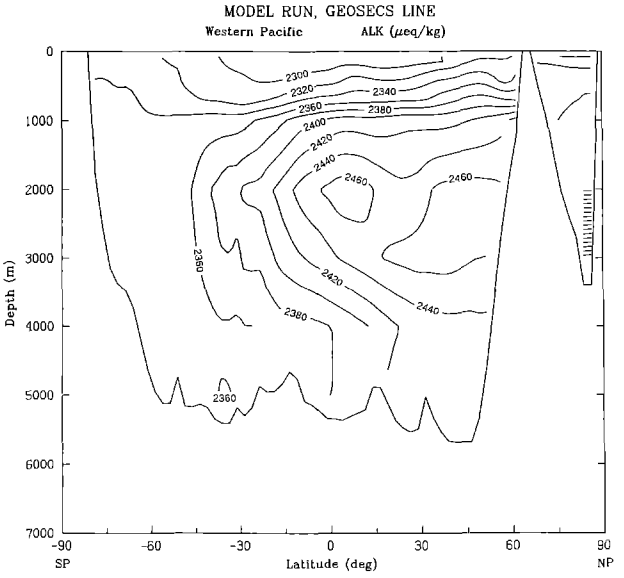

a

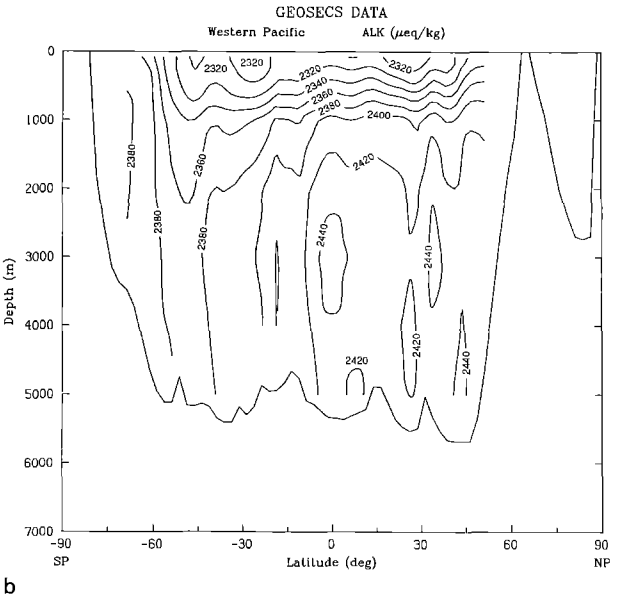

b

Fig. 31 a, b. Vertical sections of titration alkalinity (μ eq kg^{-1}) in Western Pacific Ocean: **a** model; **b** GEOSECS data

el. The diffusive parameterization employed by MRH, and described above, permits more mixing at locations where boxes are mixed more often than once per year in the circulation model. The ocean-borne fraction with this parameterization of convective mixing is increased by 0.03.

A factor not included in the model is variation of the atmosphere-ocean exchange velocity with location. Wind tunnel results combined with information on wind speeds over the ocean lead to a prediction that the exchange velocity should be expected to vary with location by approximately a factor of 3 (Erickson 1989; Heimann and Monfray 1989). However, the ocean-borne fraction is not very sensitive to the exchange velocity: a doubling of the average exchange velocity increased the model ocean-borne fraction by only 0.016.

Carbon pumps

Three mechanisms have been identified by which the vertical gradient in total CO_2 is maintained.

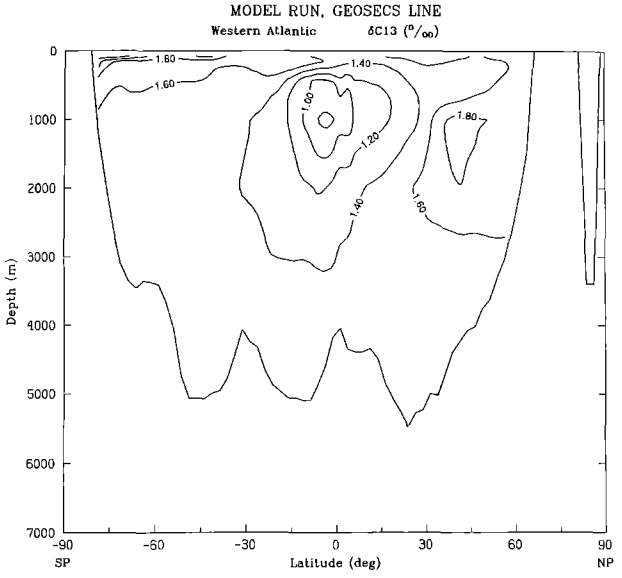

Fig. 32. Vertical section of model $\delta^{13}C$ (‰) in Western Atlantic Ocean

Volk and Hoffert (1985) refer to these as carbon pumps: the soft-tissue pump, the carbonate pump, and the solubility pump. The mechanism of the solubility pump is that the concentration of total CO_2 in newly formed deep water tends to be relatively high because deep water almost entirely forms at high latitudes, especially in the North Atlantic. Because temperatures are low in the deep water formation regions, the water there tends to have gained CO_2 from the atmosphere. The effect

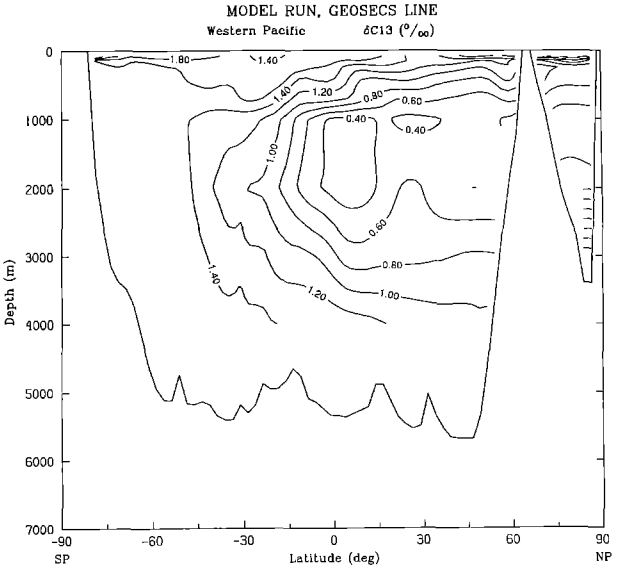

Fig. 33. Vertical section of model $\delta^{13}C$ (‰) in Western Pacific Ocean

of the carbonate pump may be eliminated from the average total CO_2 concentration in below surface water $TCO2_d$ by subtracting the carbonate effect, CAR, to give ΔCOX (Fiadeiro 1980):

$$CAR = 0.5(\mathrm{ALK}_d - \mathrm{ALK}_m + \mathrm{RN}(\mathrm{PO4}_d - \mathrm{PO4}_m)) \quad (5)$$

$$\Delta COX = \mathrm{TCO2}_d - CAR \quad (6)$$

where ALK indicates average alkalinity concentration, PO4 indicates average phosphate concentration, RN is the nitrogen to phosphate Redfield ratio (15 in the model), and the subscripts m and d refer to the surface boxes and below surface boxes, respectively. The contribution of the soft-tissue pump to the surface to bolow surface water gradient may be estimated from the difference in phosphate concentration and the carbon to phosphate Redfield ratio RC (105):

$$\Delta\mathrm{TCO2}_{soft} = RC(\mathrm{PO4}_d - \mathrm{PO4}_m). \quad (7)$$

Then the solubility pump effect can be calculated as the difference between ΔCOX and $\Delta\mathrm{TCO2}_{soft}$. In this way we find that the total CO_2 concentration difference between surface and deeper water, 240 μ mol kg^{-1}, is 21% caused by the carbonate pump, 17% caused by the solubility pump, and 62% caused by the soft-tissue pump. Volk and Hoffert estimate from GEOSECS data that in the real ocean the solubility pump contributes about 40% of the concentration difference contributed by the soft-tissue pump; in the model, this ratio is 28%. With no ocean biota, total CO_2 concentration difference between surface and deeper water is 25% of the difference with ocean biota, and must be entirely caused by the solubility pump.

Effect of reduced ocean circulation intensity

One would like to know the sensitivity of the model atmospheric CO_2 to changes in ocean circulation. This would best be done through a change in the ocean general circulation model forcing, but a start can be made by reducing all velocities together by 40%. The reduced field still conserves water and chemical species but, of course, violates the geostrophic balance somewhat. Reduced circulation is particularly interesting because there is some evidence that North Atlantic Deep Water formation was reduced during the last glacial epoch (Boyle and Keigwin 1982). The 40% reduction in circulation velocities causes atmospheric CO_2 to adjust to a new equilibrium 39 ppm lower than its starting level. The reason

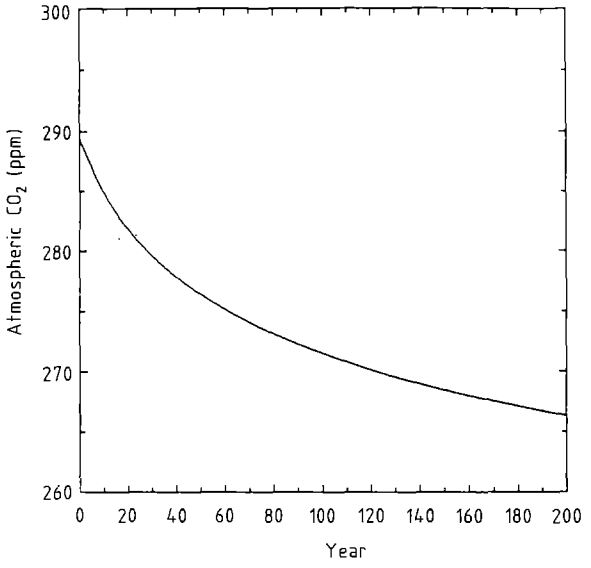

Fig. 34. Effect of suddenly reducing all ocean circulation velocities by 40%. The final equilibrium atmospheric CO_2 level is about 250 ppm. The time constant for the first 20 years of the adjustment is 84 years, after which the adjustment becomes much slower

the atmospheric CO_2 concentration falls is that the three carbon pumps discussed above have more time to reduce total CO_2 in the surface boxes relative to the time to bring in more CO_2. The surface concentration of CO_2 is determined by the balance between input and loss, so a reduction in the rate of input relative to loss causes the concentration to fall. Total new production is reduced, along with the reduction in circulation, but the percentage reduction (24%) is less than for the circulation (40%). The gradient in total CO_2 between surface and deeper water is increased by 17%; a carbon pump analysis indicates that all three pumps — soft-tissue, solubility, and carbonate — are equally strengthened by 17%. The adjustment is initially relatively rapid (Fig. 34), but then becomes slower due to the slow mixing of surface water with deeper water.

A 40% reduction in circulation velocities for a model with no biota, adjusted to near 290 ppm by varying the model total CO_2, results in a reduction in atmospheric CO_2 of 21 ppm, which compares with 39 ppm for the model with biota. Here the effect must be entirely due to the solubility pump.

Effect of ocean biota on natural radiocarbon distributions

It is useful to compare the distribution of natural $\Delta^{14}C$ in the standard case model with models with no biota. There are two of these that occur rather naturally: model B has been adjusted (by varying the model total CO_2) so that its atmosphere is close to 290 ppm, as is the standard case model, referred to here as model A; and model C which has the same total CO_2 content as the standard case model, and a much higher atmospheric CO_2 level (456 ppm). The average $\Delta^{14}C$ of the ocean carbon in model B, relative to the carbon in the atmosphere, is almost exactly the same as for the standard case model, and the $\Delta^{14}C$ ocean section contours are also nearly the same (Figs. 35 and 36, a and b). However, the ocean carbon in model C is less depleted, by about 20‰ (Figs. 35c and 36c):

Model	Biota	Total CO_2 moles	Atm CO_2 ppm	$1+\Delta^{14}C$
A	Yes	same	289	0.85
B	No	less	289	0.85
C	No	same	456	0.87

This model behavior is most easily understood by examining the corresponding behavior of the two-box ocean model. One finds that the ratio of ^{14}C to total carbon in the deep ocean box to that in the surface box is completely independent of the magnitude of the particulate flux, when fractionation coefficients are set to unity. The corresponding ratio of ^{14}C to total carbon in the surface box to that in the atmospheric box has the same form as with no particulate flux, but it involves ratios of the total carbon in the surface ocean and deep ocean to that in the atmosphere (see Keeling 1973, Eqs. 6.31 and 6.32, p 289). In model C, these ratios are approximately half as large as in models A and B.

Since $\Delta^{14}C$ contours hardly differ between models with and without biota, provided that the atmospheric CO_2 concentration is held approximately the same, we conclude that $\Delta^{14}C$ contours are insensitive to the formulation of the biota model. The fractionation correction removes the effect of the biota. This result is not contrary to the findings of MRH, as discussed below.

MRH ^{14}C distributions

MRH Figs. 11, 13, and 23, although labeled $\Delta^{14}C$, are instead $\delta^{14}C$, i.e., they were calculated with fractionation coefficients that are the square of the coefficients for ^{13}C. The use of the capital Δ

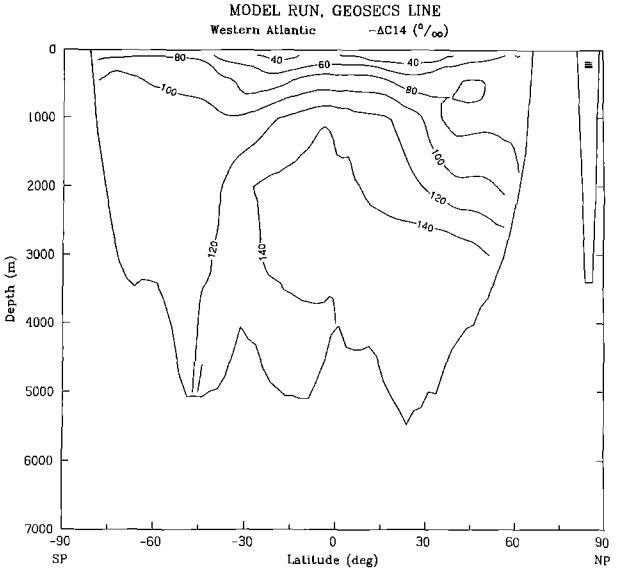

a

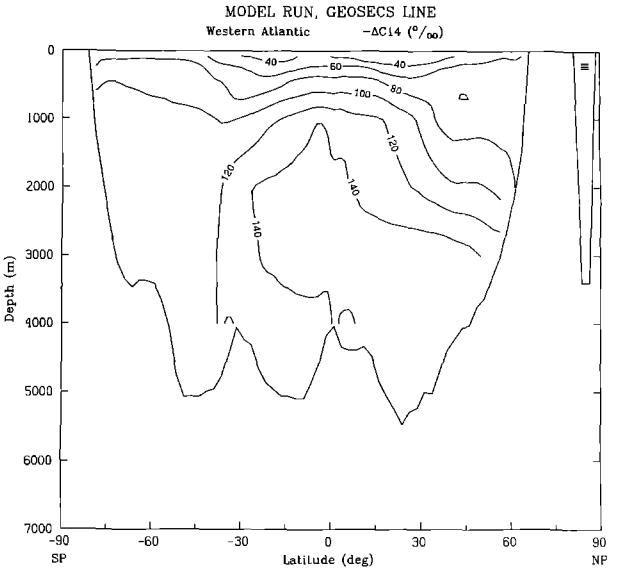

b

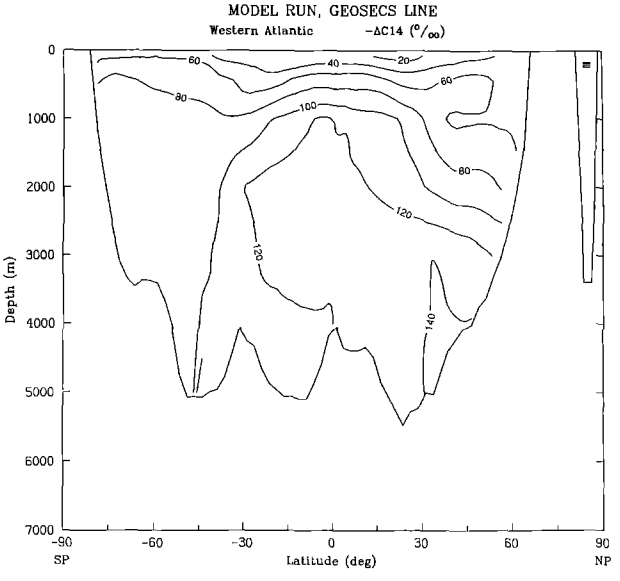

c

Fig. 35a–c. Vertical sections of pre-industrial $\Delta^{14}C$ (‰) in Western Atlantic Ocean: **a** standard case model; **b** standard case model with no biota and atmospheric CO_2 concentration adjusted to same value as standard case model; **c** standard case model with no biota, same total CO_2 in system, and higher atmospheric CO_2 concentration

has come by convention to refer to fractionation corrected values (see Keeling 1981, p 92). In modeling, this may be accomplished by setting the fractionation coefficients to unity, as has been done in the present study; or, alternatively, modeled ^{13}C values could be used to correct the modeled ^{14}C values for fractionation in the same way as is done with the measurements. The MRH ^{14}C distributions were not corrected for fractionation; consequently they are sensitive to the inclusion of the ocean biota, as indicated by a comparison of MRH Figs. 11 and 13.

Bomb radiocarbon

We find that simulated ^{14}C from the nuclear test explosions during the 1960s have not much disturbed the model contours of $\Delta^{14}C$ below about 1000 m, except in isolated regions in the North Atlantic and southern oceans (Figs. 22a and 35a, 23a and 36a).

MRH Fig. 23b and 23d show the deep waters of the ocean to be more depleted in ^{14}C by 8‰ in 1973 than 1820. This 8‰ is an error due to inconsistent use of the atmosphere as the standard.

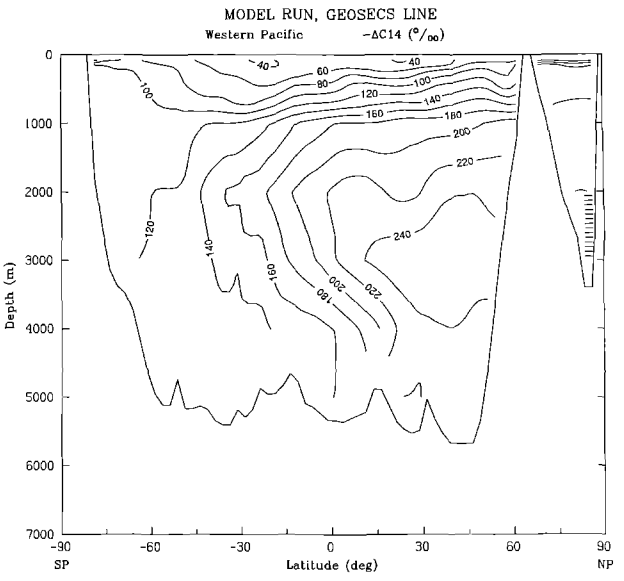

a

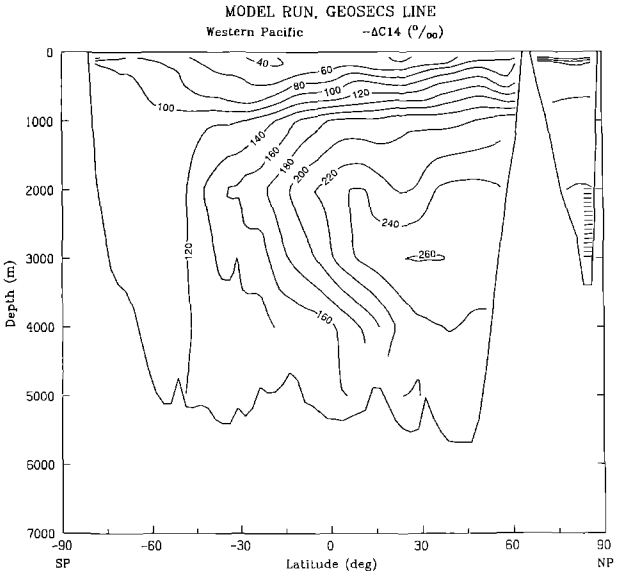

b

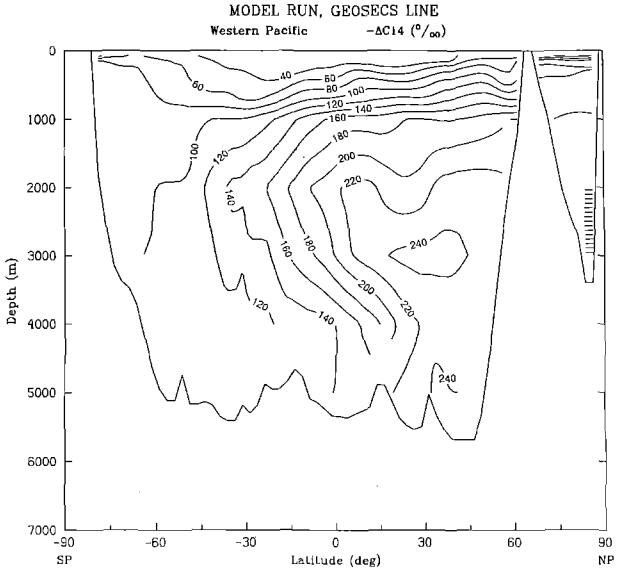

c

Fig. 36a–c. Vertical sections of pre-industrial $\Delta^{14}C$ (‰) in Western Pacific Ocean: **a** standard case model; **b** standard case model with no biota and atmospheric CO_2 concentration adjusted to same value as standard case model; **c** standard case model with no biota, same total CO_2 in system, and higher atmospheric CO_2 concentration

Conclusions

The modeled ocean is not identical to the real ocean, but it is very similar, and processes such as the formulation of the biota model can be studied effectively. The most serious shortcoming of the circulation field is that too much of the deep water formation occurs in the southern oceans relative to the North Atlantic. Ocean tracer distributions are very sensitive to deep water formation. One can expect that the ocean circulation field will improve with more development effort. The ability to spin-up the chemical model in a self-consistent way is a powerful tool for studying model formulation.

Acknowledgements. We would like to acknowledge helpful discussions with Klaus Hasselmann and C. David Keeling, and thank them for their encouragement. The work of R. Bacastow was performed for the Carbon Research Division, Office of Energy Research, under subcontract No. 19X-43386C between Scripps Institution of Oceanography and Martin Marietta Energy Systems, Inc., under contract DE-AC05-840R21400 with the U.S. Department of Energy. He also received partial support from the Max-Planck Institut for 1 year. R. Bacastow performed calculations at both the National Magnetic Fusion Computer Center and the San Diego Super Computer Center.

Appendix

Numerical scheme

The achievement of a dynamic steady state between the ocean circulation and the biota model requires numerical integration over a model time period longer than the mixing time of the model ocean. Since the mixing time of the real ocean is the order of 1000 years, conservation of chemical species becomes very important. The numerical scheme used to integrate the advective-diffusive equation conserves the mass of chemical species in the sense of Eq. (1) to a precision determined by the numerical resolution of the computer. It is not the same as the scheme used in the ocean general circulation model. The discussion below of the numerical scheme is very explicit because geochemists who might use this model would need to understand it in detail.

The advection scheme makes use of water conservation, which in the circulation model takes the form

$$\nabla \cdot \vec{\mathbf{U}} = 0, \tag{8}$$

where $\vec{\mathbf{U}}$ is the vector velocity, with components: u, positive to the east, v, positive to the north, and w, positive upward. The small variation in density has been neglected. Integration over one of the boxes into which the ocean is divided (see main text) and the application of Gauss's theorem results in

$$\int_b \vec{\mathbf{U}} \cdot d\vec{\mathbf{S}} = 0, \tag{9}$$

where $\vec{\mathbf{S}}$ is vector area, and the integral is over all the surfaces of the box b. With the notation of Fig. 37, Eq. (9) leads to:

$$v_N l_N h_N - v_S l_S h_S + u_E dh_E - u_W dh_W + (w_T - w_B) ld = 0, \tag{10}$$

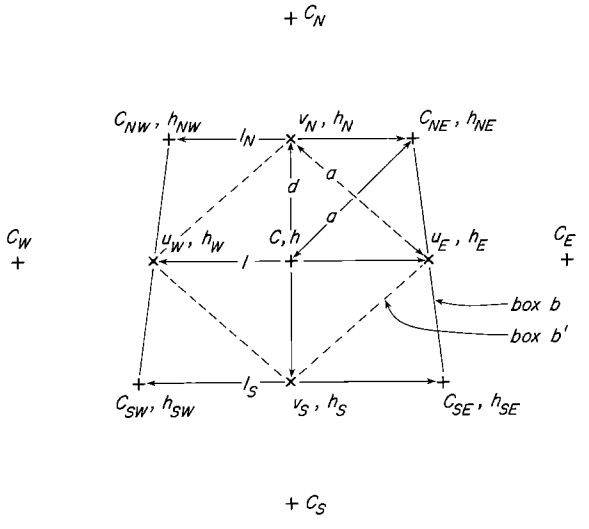

Fig. 37. Plan view of elementary box surrounding a scalar point. Notation used in the Appendix is indicated: C refers to concentration, h to box height, u and v to easterly and northerly components, respectively, of the current velocity, and d and l to the indicated box dimensions. The subscripts N, S, E, and W are compass directions from the central scalar point used to designate other points relative to the central point. Note that because of the spherical geometry, l_N and l_S differ from l in length

where w_T and w_B are at the top and bottom of the box, respectively. At the ocean surface and bottom, w is constrained to be zero.

Similarly, the advection equation for a chemical species with concentration C is

$$\frac{\partial C}{\partial t} + \nabla \cdot C\vec{\mathbf{U}} = 0. \tag{11}$$

Integration over one of the boxes as above results in

$$\frac{\partial \bar{C}}{\partial t} \Delta V_b + \int_b C\vec{\mathbf{U}} \cdot d\vec{\mathbf{S}} = 0 \tag{12}$$

where

$$\Delta V_b = ldh \tag{13}$$

is the volume of the box, and $\bar{C}$ is the average concentration in the box. To avoid a complicated notation, however, the bar above C will now be omitted. Again with the notation of Fig. 37, and following the prescription of Eq. (12), the numerical approximation for the time step Δt is taken to be

$$\begin{aligned}\left(\frac{C^n - C^0}{\Delta t}\right) ldh &+ \left(\frac{C_N^n + C^n}{2}\right) l_N h_N v_N - \left(\frac{C_S^n + C^n}{2}\right) l_S h_S v_S \\ &+ \left(\frac{C_E^n + C^n}{2}\right) dh_E u_E - \left(\frac{C_W^n + C^n}{2}\right) dh_W u_W \\ &+ \left(\frac{C_T^n + C^n}{2}\right) ldw_T - \left(\frac{C_B^n + C^n}{2}\right) ldw_B = 0\end{aligned} \tag{14}$$

where the superscripts o and n refer to values before and after the time step, respectively.

Equation (14) expresses the change in amount of the chemical species represented by **C**, in a particular box, in terms of the flux of the species across surfaces shared with neighboring boxes. Consequently, all loss from one box must add to another box, and the total amount of each species, when summed as in Eq. (1), will be conserved.

Subtraction of C^n times Eq. (10) gives:

$$\begin{aligned}\left(\frac{C^n - C^0}{\Delta t}\right) ldh &- \left(\frac{C^n - C_N^n}{2}\right) l_N h_N v_N + \left(\frac{C^n - C_S^n}{2}\right) l_S h_S v_S \\ &- \left(\frac{C^n - C_E^n}{2}\right) dh_E u_E + \left(\frac{C^n - C_W^n}{2}\right) dh_W u_W \\ &- \left(\frac{C^n - C_T^n}{2}\right) ldw_T + \left(\frac{C^n - C_B^n}{2}\right) ldw_B = 0.\end{aligned} \tag{15}$$

With the addition of the left-hand side of (15) above of

$$\begin{aligned}\left(\frac{C^n - C_N^n}{2}\right) l_N h_N |v_N| &+ \left(\frac{C^n - C_S^n}{2}\right) l_S h_S |v_S| \\ &+ \left(\frac{C^n - C_E^n}{2}\right) dh_E |u_E| + \left(\frac{C^n - C_W^n}{2}\right) dh_W |u_W| \\ &+ \left(\frac{C^n - C_T^n}{2}\right) ld|w_T| + \left(\frac{C^n - C_B^n}{2}\right) ld|w_B|\end{aligned} \tag{16}$$

the terms of which cancel in pairs when summed over all the boxes, a simple "up-stream" advection scheme is obtained that conserves chemical species:

$$\frac{C^n - C^o}{\Delta t} + \left(\frac{C^n - C^n_N}{d}\right)\frac{l_N}{l}\frac{h_N}{h}\left(\frac{|v_N| - v_N}{2}\right) + \left(\frac{C^n - C^n_S}{d}\right)\frac{l_S}{l}\frac{h_S}{h}\left(\frac{|v_S| + v_S}{2}\right) + \left(\frac{C^n - C^n_E}{l}\right)\frac{h_E}{h}\left(\frac{|u_E| - u_E}{2}\right) + \left(\frac{C^n - C^n_W}{l}\right)\frac{h_W}{h}\left(\frac{|u_W| + u_W}{2}\right) + \left(\frac{C^n - C^n_T}{h}\right)\left(\frac{|w_T| - w_T}{2}\right) + \left(\frac{C^n - C^n_B}{h}\right)\left(\frac{|w_B| + w_B}{2}\right) = 0. \quad (17)$$

The above scheme is an implicit scheme since the concentrations C^n are not known until after the time step. Implicit schemes are unconditionally stable, which permits a large time step, although they may be inaccurate particulary if concentrations change rapidly.

To find the C^n, the solution of a large number of linear equations is required at each time step. It has been found possible to solve these equations iteratively. For this iteration, (17) is written

$$C^{n,i+1}(1 + F_N + F_S + \ldots F_B) = C^o + F_N C^{n,i}_N + F_S C^{n,i}_S + \ldots F_B C^{n,i}_B \quad (18)$$

where

$$F_N = \frac{\Delta t}{d}\frac{l_N}{l}\frac{h_N}{h}\left(\frac{|v_N| - v_N}{2}\right) \quad (19)$$

is the coefficient of C^n_N in Eq. (17), after multiplying both sides by Δt, and similarly for $F_S \ldots F_B$. The additional superscript i indicates the iteration level.

With the simple up-stream advection scheme described above, a checkerboard solution would be expected because the scheme operates independently in the two oceans that the scalar points define. To avoid this, horizontal diffusion is introduced so as to connect the two sets of scalar points.

The diffusion equation is

$$\frac{\partial C}{\partial t} = \nabla \cdot (K \nabla C). \quad (20)$$

A (diamond-shaped) box b' is defined around each scalar point by taking the corners to be at the four surrounding vector points (see Fig. 37), with the depth of the box as before. Integration of (20) over one of these boxes results in

$$\frac{\partial C}{\partial t}\Delta V_{b'} = \int_{b'} K \nabla C \cdot d\vec{\mathbf{S}} \quad (21)$$

where

$$\Delta V_{b'} = \frac{ldh}{2}. \quad (22)$$

It is necessary now to choose a height for each of the four sides of the box b' through which diffusion will be supposed to take place; we have chosen to use the average of the heights at the two vector points that define each side because this choice prevents diffusive exchange between a "wet" point and an adjacent "dry" point in a natural way — both these heights will be zero if one of the points is "dry". Following (21), and with constant K, a central difference numerical scheme is obtained:

$$\frac{C^n - C^o}{\Delta t} = \frac{2K}{dlh}\left[\left(\frac{C^n_{NE} - C^n}{a}\right)a\left(\frac{h_N + h_E}{2}\right) + (C^n_{SW} - C^n)\left(\frac{h_S + h_W}{2}\right) + (C^n_{SE} - C^n)\left(\frac{h_S + h_E}{2}\right) + (C^n_{NW} - C^n)\left(\frac{h_N - h_W}{2}\right)\right]. \quad (23)$$

Note that the length of the side of box b', a in Fig. 37, cancels between the distance parameter in the formulation of the gradient and the area over which diffusion is assumed to take place.

Diffusion is actually included with the implicit advection scheme, i.e.

$$\text{total}\ \frac{C^n - C^o}{\Delta t} = \text{r.h.s. (17)} + \text{r.h.s. (23)} \quad (24)$$

where r.h.s. abbreviates "right-hand side". A time step then consists of an adjustment of concentrations according to biota and atmospheric exchanges, and the convective adjustment (see text), followed by an advective-diffusive step. The iteration scheme for the advective-diffusive step begins with concentrations C set to their values at the end of the preceding time step, before the exchanges and convective adjustment of the new time step. If the iteration scheme begins with adjusted concentrations, convergence is much slower. Ordinarily, 4 iterations were made.

Conservation of chemical species in the advective-diffusive step depends on convergence of the iteration procedure; if convergence is incomplete, terms in Eq. (17), which should cancel in a sum over all boxes as in Eq. (1), will involve concentrations at different degrees of convergence and fail to completely cancel. An explicit advection-diffusion scheme based on the above equations would be expected to conserve mass absolutely, within the numerical precision of the calculation, but then a very short time step would be required for stability. An explicit scheme uses only concentrations before the time step, so there is no iteration required.

A "spin-up" run was ordinarily for 2400 model years with a time step of 1 year and required about 35 min of time on a single Cray processor. With addition of fossil fuel, it was found necessary to reduce the time step to ¼ year, or a significant amount of fossil fuel CO_2 would be lost. Then, with the convective adjustment made only once per year, there would be larger concentration adjustments during the time step of the convective adjustment and also during the following time step, so for these two time steps, the number of iterations was doubled to 8. With diffusive parameterization of convection, as done by (MRH) (see text), this increase in the number of iterations with reduced time step was unnecessary.

Some tests were made with the biological source/sink, atmospheric exchange, and convective adjustment all based on "new" values and included in the iteration loop of the advection scheme, as called for by the implicit prescription with fossil fuel input. This more complicated procedure is not as important during "spin-up" because then stationary values of the concentrations are sought. However, the program then became 25% larger and took twice as long to run. With the time step reduced to ¼ year, the difference between the two procedures became very small, and it was decided just to reduce the time step.

References

Arakawa A, Lamb VR (1977) Computational design of the basic dynamical processes of the UCLA general circulation model. Methods Comput Phys 17:173–265

Bacastow RB (1981) Numerical evaluation of the evasion factor. In: Bolin B (ed) Scope 16: Carbon cycle Modelling. John Wiley, New York, pp 95–101

Bacastow R, Björkström A (1981) Chapter 2: Comparison of ocean models for the carbon cycle. In: Bolin B (ed) Scope 16: Carbon cycle modelling. John Wiley, New York

Bacastow R, Maier-Reimer E (1990) Modeling oceanic new production. In: Keir R (ed) Interaction of the global carbon and climate systems. Electric Power Research Institute Report (in press)

Bainbridge AE (undated) GEOSECS Atlantic expedition, Volume 2, Sections and profiles. US Government Printing Office, Washington, DC 20402, Stock No. 038-000-00435-2

Bathen KH (1972) On the seasonal changes in the depth of the mixed layer in the North Pacific Ocean. J Geophys Res 77:7138–7150

Berger WH, Fischer K, Lai C, Wu G (1987) Ocean productivity and organic carbon flux, Part I: Overview and maps of primary production and export production, SIO Ref. 87-30. Univ. Calif., San Diego, La Jolla; also Berger WH (1989) Appendix: Global maps of ocean productivity. In Berger WH, Smetacek VS, Wefer G (eds) Productivity in the ocean, present and past. John Wiley, New York, pp 429–455

Boyle EA, Keigwin LD (1982) Deep circulation of the North Atlantic over the last 200000 years: geochemical evidence. Science 218:784–787

Brewer PG (1986) What controls the variability of carbon dioxide in the surface ocean? A plea for complete information. In: Burton JD, Brewer PG, Chesselet R (eds) Dynamic Processes in the Chemistry of the Upper Ocean. Plenum Press New York, pp 215–231

Brewer PG, Wong GTF, Bacon MP, Spencer DW (1975) An oceanic calcium problem? Earth Plant Sci Lett 26:81–87

Broecker WS, Peng T-H (1982) Tracers in the sea. Lamont-Doherty Geological Observatory, Palisades, New York, 691 p

Chen CTA, Feely RA, Gendron JF (1988) Lysocline, calcium carbonate compensation depth and calcareous sediments in the North Pacific Ocean, Contribution No. 974. NOAA/Pacific Marine Environmental Laboratory

Clarke RA (1985) Temporal and spatial scales of Laborador sea water formation. In: Bennett T, Broecker W, Hansen J (eds) North Atlantic deep water formation. NASA Conference Publication 2367, pp 7–11

Craig H, Broecker WS, Spenser D (1981) GEOSECS Pacific expedition, volume 4, sections and profiles. U.S. Government Printing Office, Washington, D. C. 20402

Defant A (1961) Physical oceanography, Vol. I. Pergamon Press, New York, pp 56–59

Delmas RJ, Ascencio JM, Legrand M (1980) Polar ice evidence that atmospheric CO_2 20000 yr BP was 50% of present. Nature 284:155–159

Detwiler RP, Hall CAS (1988) Tropical forests and the global carbon cycle. Science 239:42–47

De Vooys CGN (1979) Primary production in aquatic environments. In Scope 13: Bolin B, Degens ET, Kempe S, Ketner P (eds) The global carbon cycle. John Wiley & Son, New York, pp 259–292

Dickson AG, Millero FJ (1987) A comparison of the equilibrium constants for the dissociation of carbonic acid in sea water media, Deep Sea Res 34:1733–1743

Druffel EM (1980) Radiocarbon in annual coral rings of Florida and Belize, Radiocarbon 22:363–371

Druffel EM (1981) Radiocarbon in annual coral rings from the eastern tropical Pacific Ocean, Geophys Res Lett 8:59–62

Druffel EM, Linick TW (1978) Radiocarbon in annnual coral rings of Florida, Geophys Res Lett 5:913–916

Druffel EM, Suess HE (1983) On the radiocarbon record in banded corals: exchange parameters and net transport of $^{14}CO_2$ between atmosphere and surface ocean. J Geophys Res 88:1271–1280

Dugdale RC (1967) Nutrient limitation in the sea: dynamics, identification and significance, Limn. Oceanogr 12:685–695

Eppley RW, Peterson BJ (1979) Particulate organic matter flux and planktonic new production in the deep ocean. Nature 282:677–680

Erickson DJ III (1989) Variations in the global air-sea transfer velocity field of CO_2. Gobal Biogeochemical Cycles 3:37–41

Fiadeiro M (1980) Carbon cycling in the ocean. In: Falkowski PG (ed) Primary productivity in the sea. Plenum Press, New York, pp 487–495

Friedli H, Lötscher H, Oeschger H, Siegenthaler U, Stauffer B (1986) Ice core record of the $^{13}C/^{12}C$ ratio of atmospheric CO_2 in the past two centuries. Nature 324:237–238

Gieskes WWC, Kraay GW, Baars MA (1979) Current ^{14}C methods for measuring primary production: gross underestimates in oceanic waters. Neth J Sea Res 13:58–78

Hasselmann K (1982) An ocean model for climate variability studies. Prog Oceanogr 11:69–92

Heimann M, Monfray P (1990) Spatial and temporal variations of the gas-exchange coefficient for CO_2: 1. Data analysis. Geophys Res (in press)

Holtslag AAM, Ulden AP van (1983) A simple scheme for daytime estimates of the surface fluxes from routine weather data. J Climate and App Met 22:517–529

Honjo S, Manganini SJ, Cole J (1982) Sedimentation of biogenic matter in the deep ocean. Deep Sea Research 29:609–625

Houghton RA, Hobbie JE, Melillo JM, Moore B, Peterson BJ, Shaver GR, Woodwell GM (1983) Changes in the carbon content of terrestrial biota and soils between 1860 and 1980: a net release of CO_2 to the atmosphere. Ecological Monographs 53(3):235–262

Jenkins WJ (1982) Oxygen utilization rates in the North Atlantic subtropical gyre and primary productivity in oligotrophic systems. Nature 300:246–248

Keeling CD (1968) Carbon dioxide in surface waters. 4. Global distributon. J Geophys Res 73:4543–4553

Keeling CD (1973) The carbon dioxide cycle: reservoir models to depict the exchange of atmospheric carbon dioxide with the oceans and land plants. In: Rasool SI (ed) Chemistry of the lower atmosphere. Plenum Press, pp 251–329

Keeling CD (1981) The modeling of rare isotopic carbon with regard to notations. In Scope 16: Bolin B (ed) Carbon cycle modelling. John Wiley & Sons, New York, pp 89–94

Keeling CD, Piper SC, Heimann M (1989) A three dimensional model of atmospheric CO_2 transport based on observed winds: 4. Mean annual gradients and interannual variations. In: Aspects of climate variability in the pacific and the Western Americas. American Geophysical Union Monograph, pp 305–363

Knox F, McElroy MB (1984) Changes in atmospheric CO_2: influence of marine biota at high latitude. J Geophys Res 89:4629–4637

Koblentz-Mishke OL, Volkovinsky VV, Kabanova JG (1970) Plankton primary production of the world ocean. Scientific exploration of the south pacific, Book No. 309-01755-6. National Academy of Sciences, Washington, D. C., pp 183–193

Kroopnick PM (1985) The distribution of ^{13}C of ΣCO_2 in the world oceans. Deep Sea Research 32:57–84

Kroopnick PM, Margolis SV, Wong CS (1977) $\delta^{13}C$ variations in marine carbonate sediments as indicators of the CO_2 balance between the atmosphere and oceans. In: Andersen NR, Malahoff A (eds) The fate of fossil fuel CO_2 in the oceans. Plenum Press, New York, pp 295–321

Maier-Reimer E, Hasselmann K (1987) Transport and storage of CO_2 in the ocean — an inorganic ocean-circulation carbon cycle model. Climate Dynamics 2:63–90

Maier-Reimer E, Hasselmann K, Olbers D, Willebrand J (1982) An ocean circulation model for climate variability studies. Technical Report, Max-Planck-Institut für Meteorologie, Hamburg, Germany

Mook WG, Bommerson JC, Staverman WH (1974) Carbonate isotope fractionation between dissolved bicarbonate and gaseous carbon dioxide. Earth and Planet Lett 22:169–176

Neftel A, Oeschger H, Schwander J, Stauffer B, Zumbrunn R (1982) Ice core sample measurements give atmospheric CO_2 content during the past 40000 yr. Nature 295:220–223

Nozaki Y, Rye DM, Turekian KK, Dodge RE (1978) A 200-year record of carbon-13 and carbon-14 variations in Bermuda coral, Geophys Res Lett 5:825–828

Oeschger H, Siegenthaler U, Schotterer U, Gugelmann A (1975) A box diffusion model to study the carbon dioxide exchange in nature. Tellus 27:168–192

Östlund HG, Stuiver M (1980) GEOSECS Pacific radiocarbon. Radiocarbon 22:25–53

Peng T-H, Broecker WS (1987) C/P ratios in marine detritus. Global Biogeochemical Cycles 1:155–161

Radach G, Maier-Reimer E (1975) The vertical structure of phytoplankton growth dynamics — a mathematical model. Mémoires Société Royal des Sciences de Liége, 6e série, tome VII, pp 113–146

Reid JL, Brinton E, Fleminger A, Venrick EL, McGowan JA (1978) Ocean circulation and Marine Life. In: Charnock H, Deacon G (eds) Advances in oceanography. Plenum Press, New York, pp 65–130

Rotty RM (1987) A look at the 1983 CO_2 emissions from fossil fuels (with preliminary data for 1984). Tellus 39B:203–208

Sarmiento JL, Toggweiler JR (1984) A new model for the role of the oceans in determining atmospheric pCO_2. Nature 308:621–624

Schulenberger E, Reid JL (1981) The Pacific oxygen maximum, deep chlorophyll maximum, and primary production, reconsidered. Deep Sea Res 28A:901–919

Siegenthaler U (1983) Uptake of excess CO_2 by an outcrop-diffusion model of the ocean. J Geophys Res 88:3599–3608

Siegenthaler U, Münnich KO (1981) $^{13}C/^{12}C$ fractionation during CO_2 transfer from air to sea. In Scope 16: Bolin B (ed) Carbon cycle modelling. John Wiley & Sons, New York, pp 249–257

Siegenthaler U, Wenk Th (1984) Rapid atmospheric CO_2 variations and ocean circulation. Nature 308:624–626

Spenser D, Broecker WS, Craig H, Weiss RF (1982) GEOSECS Indian ocean expedition, volume 6, sections and profiles. US Government Printing Office, Washington, DC 20402

Stuiver M, Östlund HG (1980) GEOSECS Atlantic radiocarbon. Radiocarbon 22:1–24

Stuiver M, Östlund HG (1983) GEOSECS Indian ocean and mediterranean radiocarbon. Radiocarbon 25:1–29

Stuiver M, Östlund HG, McConnaughey TA (1981) GEOSECS Atlantic and pacific ^{14}C distribution. In Scope 16: Bolin B (ed) Carbon Cycle modelling. John Wiley & Sons, pp 201–226

Takahashi T, Broecker WS, Bainbridge AE (1981a) Supplement to the alkalinity and total carbon dioxide concentration in the World Oceans. In Scope 16: Bolin B (ed) Carbon cycle modelling. John Wiley & Sons, pp 159–199

Takahashi T, Broecker WS, Bainbridge AE (1981b) The alkalinity and total carbon dioxide concentration in the World Oceans. In Scope 16: Bolin B (ed) Carbon cycle modelling. John Wiley & Sons, pp 271–286

Takahashi T, Broecker WS, Langer S (1985) Redfield ratio based on chemical data from isopycnal surfaces. J Geophys Res 90:6907–6924

Takahashi T, Chipman D, Volk T (1983) Geographical, seasonal, and secular variations of the partial pressure of CO_2 in surface waters of the North Atlantic Ocean: the results of the North Atlantic TTO program, II.123–II.145. In: Proceedings of carbon dioxide research conference: carbon dioxide, science and consensus, Sept. 19–23, 1982, Berkeley Springs, West Virginia, USA, CONF-820970, US Dept of Energy, Washington DC, available from NTIS, Springfield, Va., USA

Tans P (1981a) A compilation of bomb ^{14}C data for use in global carbon model calculations. In Scope 16: Bolin B (ed) Carbon cycle modelling. pp 131–157

Tans P (1981b) $^{13}C/^{12}C$ of industrial CO_2. In Scope 16: Bolin B (ed) Carbon cycle modelling. John Wiley & Sons, New York, pp 127–129

Volk T, Hoffert MI (1985) Ocean carbon pumps: analysis of relative strengths and efficiencies in ocean-driven atmospheric CO_2 changes. In: Sundquist ET, Broecker WS (eds) The carbon cycle and atmospheric CO_2: Natural variations archean to present. American Geophysical Union, Washington, DC, pp 99–110

Volk T, Liu Z (1988) Controls of CO_2 sources and sinks in the earthscale surface ocean: temperature, nutrients. Global Biogeochemical Cycles 2:73–89

Walsh JJ (1975) A spatial simulation model of the Peru upwelling ecosystem. Deep Sea Res 22:201–236

Weiss RF (1970) The solubility of nitrogen, oxygen, and argon in water and sea water. Deep Sea Res 17:721–735

Weiss RF (1974) Carbon dioxide in water and sea water: The solubility of a non-ideal gas. Marine Chem 2:203–215

Wroblewski JS (1977) A model of phytoplankton plume formation during variable Oregon upwelling. J Marine Res 35-2:357–394